

THE RUNAWAYS AND ISOLATED O-TYPE STAR SPECTROSCOPIC SURVEY OF THE SMC (RIOTS4)*

J. B. LAMB^{1,2}, M. S. OEY¹, D. M. SEGURA-COX^{1,3}, A. S. GRAUS^{1,4}, D. C. KIMINKI⁵, J. B. GOLDEN-MARX¹,
AND J. WM. PARKER⁶

***Accepted for publication in ApJ ***

ABSTRACT

We present the Runaways and Isolated O-Type Star Spectroscopic Survey of the SMC (RIOTS4), a spatially complete survey of uniformly selected field OB stars that covers the entire star-forming body of the SMC. Using the IMACS multislit spectrograph and MIKE echelle spectrograph on the Magellan telescopes, we obtained spectra of 374 early-type field stars that are at least 28 pc from any other OB candidates. We also obtained spectra of an additional 23 field stars in the SMC bar identified from slightly different photometric criteria. Here, we present the observational catalog of stars in the RIOTS4 survey, including spectral classifications and radial velocities. For three multi-slit fields covering 8% of our sample, we carried out monitoring observations over 9–16 epochs to study binarity, finding a spectroscopic, massive binary frequency of at least $\sim 60\%$ in this subsample. Classical Oe/Be stars represent a large fraction of RIOTS4 (42%), occurring at much higher frequency than in the Galaxy, consistent with expectation at low metallicity. RIOTS4 confirmed a steep upper IMF in the field, apparently caused by the inability of the most massive stars to form in the smallest clusters. Our survey also yields evidence for in-situ field OB star formation, and properties of field emission-line star populations, including sgB[e] stars and classical Oe/Be stars. We also discuss the radial velocity distribution and its relation to SMC kinematics and runaway stars. RIOTS4 presents a first quantitative characterization of field OB stars in an external galaxy, including the contributions of sparse, but normal, star formation; runaway stars; and candidate isolated star formation.

Subject headings: galaxies: Magellanic Clouds – galaxies: stellar content – stars: early-type – stars: emission-line, Be – stars: fundamental parameters – binaries: spectroscopic – stars: kinematics

1. INTRODUCTION

The standard model of star formation has been that most, if not all, stars form in clusters (e.g., Lada & Lada 2003), with the most massive stars aggregating in the dense cores of clusters. It is intuitive that massive O stars form preferentially from the plentiful gas reservoirs of giant molecular clouds (GMCs). However, another significant population of massive stars exists in an environment of the opposite extreme. These massive stars are far removed from dense clusters or OB associations and instead appear isolated within the sparse field population. The physical properties and origin of this field massive star population remain unclear, despite the fact that it accounts for 20–30% of the massive stars in star-forming galaxies (Oey et al. 2004). The existence of such stars in isolation poses a challenge for theories of massive star formation, which suggest that the necessary gas conditions are primarily or exclusively found in GMCs. Alternatively, rather than having formed in the field, these stars

may have formed in clusters, and then been subsequently ejected from their birth locations as runaway stars. In either case, field massive stars are a unique, understudied subset of a galaxy’s massive star population, probing both extremely sparse and extremely dense star-forming conditions.

The observational evidence for in situ field massive star formation has grown in recent years. An optical and UV photometric census of candidate O-type stars in a portion of the LMC suggests that approximately half of these stars may be members of the field population (Parker et al. 2001). Some strong, direct evidence of formation in the field is work by Testi et al. (1997, 1998), who reported a sample of Herbig Ae/Be stars forming in isolation. At higher masses, Lamb et al. (2010) detected sparse clusters associated with field OB stars in the Small Magellanic Cloud, and Bressert et al. (2012) identified 15 O stars that are candidates for isolated formation near 30 Doradus, based on a variety of criteria. Additional individual candidates have been reported by Selier et al. (2011) and Oskinova et al. (2013). Oey et al. (2013) presented a sample of 14 field OB stars centered in circular HII regions, thus implying that they are unlikely to have transverse runaway velocities. Since these objects furthermore have non-runaway radial velocities, they most likely formed in situ. This growing observational dataset of massive stars that appear to have formed in sparse clusters or in isolation, without any indication of being runaways, strongly suggests that some component of the field massive star population formed in situ. Even so, formation within clusters cannot be entirely ruled out

* This paper includes data gathered with the 6.5 meter Magellan Telescopes located at Las Campanas Observatory, Chile.

¹ Astronomy Department, University of Michigan, 1085 S. University Ave., Ann Arbor, MI 48109-1107

² Department of Physical Sciences, Nassau Community College, One Education Drive, Garden City, NY 11530

³ Department of Astronomy, University of Illinois, Urbana, IL 61801

⁴ Department of Physics and Astronomy, University of California, Irvine, CA 92697

⁵ Department of Astronomy, University of Arizona, Tucson, AZ 85721

⁶ Southwest Research Institute, Department of Space Studies, Suite 300, 1050 Walnut Street, Boulder, CO 80302-5150, USA

for these stars. Gvaramadze et al. (2012) point out that cluster dissolution, slow ejections, or multi-stage ejections could all potentially mask the signatures that these stars formed in clusters.

This problem on the origin of field OB stars is central to some outstanding controversies. Weidner & Kroupa (2006) suggest a deterministic relation between cluster mass and the associated maximum stellar mass; whereas if it is indeed the case that massive stars can form in sparse, low-mass clusters, it would suggest a large dispersion in the relation between cluster mass and the associated maximum stellar mass, which is inconsistent with such a scenario. Furthermore, it would also imply that individual sparse clusters must necessarily have stellar initial mass functions (IMFs) that grossly deviate from any standard values. It remains unclear whether such deviations are real or whether they arise from stochastic sampling, so that an aggregate population of sparse clusters would yield a Salpeter-like IMF, as suggested by Lamb et al. (2010).

These issues are simply a consequence of the difficulties in understanding sparse massive star formation within the framework of current star formation models. Two primary theories for massive star formation are the competitive accretion model and the core accretion model. In the competitive accretion model, molecular clouds fragment into star forming cores, which continue to accrete matter from a shared reservoir of gas. In this scenario, massive stars form in locations where the gas density is highest, which is typically in the centers of GMCs (Zinnecker 1982). Thus, it is implicit to the competitive accretion model that massive stars may only form along with a significant population of lower mass stars (Bonnell et al. 2004). In contrast, core accretion models suggest that the gas available for accretion is controlled by the mass of the fragmented core itself (Shu et al. 1987). Thus in core accretion models it is possible, although difficult, to obtain gas conditions that would allow a massive star to form in isolation (e.g. Krumholz et al. 2009).

A less controversial component of the field is the runaway population. Observationally, isolated massive stars with large space velocities are well-known to exist. The typical definition for runaway stars is a peculiar space velocity $> 30 \text{ km s}^{-1}$. Using this definition, runaway fractions ranging from 10% (Blaauw 1961) to 50% (de Wit et al. 2005) have been observed for massive stars within the Galaxy. However, other studies use evidence from bow shocks, the likelihood of slow runaway ejections, and the possibility of exotic multi-stage ejection mechanisms to suggest that the true runaway fraction is much higher, up to 100% of the field population (Gvaramadze et al. 2012). In this scenario, the field population is comprised primarily of stars that formed in dense cluster cores, where the best conditions for massive star ejections exist. Thus, the field population is a vital probe of the massive star formation process at both the densest and least dense extremes.

Other than the obvious kinematic signatures expected for runaway stars, it is not well known how the properties of massive stars formed in isolation vs runaways would differ from stars in clusters. Observational studies do reveal a few trends: for example, a study by van den Bergh (2004) compares the distribution of spectral types be-

tween field and cluster O stars within the magnitude-limited Galactic O Star Catalog (Maíz-Apellániz et al. 2004), finding that spectral types for field stars are skewed toward later types than stars in clusters. Thus, field O stars are either older or less massive as a population than O stars in clusters. A similar result was found in the Magellanic Clouds, where Massey et al. (1995) and Massey (2002) discovered that the field population has an extremely steep IMF in a few selected fields. The stellar IMF for stars in clusters is generally consistent with the classical Salpeter slope of $\Gamma = 1.35$ for a power law given by $dn/d\log m \propto m^{-\Gamma}$, where n is the number of stars of mass m . However, Massey et al. (1995) found a high-mass field IMF slope of $\Gamma \sim 4$ using a combination of spectra and photometry. This steep IMF also suggests that field massive stars are typically less massive than the massive stars in clusters. These findings represent the largest systematic departure from a Salpeter IMF based on direct star counts, and suggest that field massive stars as a population may originate in a fundamentally different way than those in clusters.

Thus, there is a clear need for a systematic, statistically complete survey of field massive stars. Unlike stars in clusters, field massive stars in the Galaxy are distributed in all directions. Together with distance uncertainties and line-of-sight confusion caused by large and differential extinction, this causes great difficulty in identifying a complete, uniformly selected sample of Galactic field O stars. Sample size and stochasticity are also issues within the Galaxy, since we are limited to sampling only the nearby Galactic field.

In order to mitigate these issues, we targeted the nearby Small Magellanic Cloud (SMC) to obtain a uniform, spectroscopic survey of its field massive star population, which we call the Runaways and Isolated O-Type Star Spectroscopic Survey of the SMC, or RIOTS4. Since the SMC is located at high Galactic latitude, it is relatively free from the line-of-sight issues that plague Galactic studies. Additionally, since all objects are at the SMC distance, RIOTS4 avoids issues associated with distance uncertainties. Thus, the most important benefit is that RIOTS4 targets a *spatially complete* and statistically significant sample of uniformly selected field massive stars. Here, we present an overview of the RIOTS4 survey and the results to date.

2. RIOTS4 TARGETS AND OBSERVATIONS

RIOTS4 targets a spatially complete sample of 374 uniformly selected candidate field OB stars in the SMC. Our targets are identified by Oey et al. (2004; hereafter OKP04) according to the photometric criteria $B \leq 15.21$ and $Q_{UBR} \leq -0.84$, where the reddening-free parameter Q_{UBR} is given by,

$$\begin{aligned} Q_{UBR} &= (U - R) - \frac{A_U - A_R}{A_B - A_R} (B - R) \\ &= (U - R) - 1.396(B - R), \end{aligned} \quad (1)$$

where the A values correspond to extinction in the specified bands. In the calculation of Q_{UBR} , OKP04 adopted the ratio of total to selective extinction $R_V = 3.1$ from Cardelli et al. (1989). These photometric criteria were designed to select stars with masses $\gtrsim 10 M_\odot$, using the B magnitude to eliminate less massive main sequence

stars, and the Q_{UBR} criterion to identify only the bluest stars; this corresponds to approximate spectral types of B0 V, B0.5 I, and earlier. OKP04 applied these criteria to the $UBVR$ photometric survey data for the SMC obtained by (Massey 2002), which was optimized to identify OB star candidates. This survey basically covered the full star-forming expanse of the galaxy, which ensures uniform selection of a spatially complete sample of massive stars in the SMC. OKP04 further carried out a friends-of-friends analysis on this sample to identify clusters. In this algorithm, stars are considered cluster members if their projected distances to other cluster members are smaller than the given clustering length. The clustering length is the value that maximizes the number of identified clusters (Battinelli 1991), which is 28 pc for the SMC sample. Thus the field OB targets for the RIOTS4 survey correspond to all candidates from the OKP04 sample with no other candidates within a 28 pc radius.

OKP04 also identified a sample of candidate field O stars in a smaller region, covering the SMC bar, using UV photometry from the *Ultraviolet Imaging Telescope* (UIT) (Parker et al. 1998). These 91 field O star candidates were selected using reddening-free indices that include UV and $UBVR$ photometry, along with the same B magnitude criteria as the main sample. Of these 91 stars, there are 23 that were not identified by the optical photometric criteria above. We included these stars in our multi-object observations as described below.

We observed the RIOTS4 survey targets over a five-year period from 2006 September to 2011 October using spectrographs on the Magellan telescopes at Las Campanas Observatory. The majority of our observations were obtained with the Inamori-Magellan Areal Camera and Spectrograph (IMACS) in the f/4 multi-slit mode on the Magellan Baade telescope (Bigelow & Dressler 2003). With 49 slit masks, we observed 328 of the 374 candidate field OB stars, or over 7/8 of our total sample. We also observed the 23 objects unique to the UV-selected sample with this setup. We used the 1200 lines/mm grating and slit widths of either $0.7''$ or $1.0''$, yielding spectral resolutions of $R \sim 3700$ and $R \sim 2600$, respectively. Due to the varying placement of slits within the slit masks, our spectral coverage for each star varies; however, every spectrum includes coverage from 4000 – 4700 Å. We observed each field for a total of one hour in three exposures of 20 minutes each, which allows us to achieve a $S/N > 30$ for our fainter targets. All observations in our IMACS multi-object campaign occurred between 2006 September to 2010 December. During our initial observing run in 2006 September one of our 49 fields was observed with the 600 lines/mm grating, resulting in a spectral resolution of $R \sim 1900$.

To maximize the multi-object fields, we were unable to include 46 of our RIOTS4 targets in the IMACS slit masks. We therefore observed these targets individually or in pairs using long slit observations. The majority of our remaining targets were observed using the Magellan Inamori Kyocera Echelle (MIKE) Spectrograph on the Magellan Clay telescope (Bernstein et al. 2003). We also used MIKE to re-observe 29 targets in cases where important diagnostic absorption lines fell within the IMACS CCD chip gaps, or when a spectrum from a multi-object

observation fell into the center gap of the IMACS CCD array. We observed a total of 48 targets with MIKE using a $1''$ slit width for a spectral resolution of $R \sim 28000$. Exposure times for MIKE observations ranged from 15 – 30 minutes depending on the brightness of the target, again with a goal of achieving $S/N > 30$. All MIKE observations occurred in 2010 November. With IMACS f/4 out of commission during our 2011 observations, we also operated IMACS in f/2 mode with a 300 lines/mm grism to observe a total of 27 objects. Depending on the seeing, we used either a $0.5''$ or $0.7''$ slit width, which yield spectral resolutions of $R \sim 1000$ and $R \sim 1300$, respectively. As in the primary IMACS campaign, we observed objects for a total of one hour, in three 20-minute exposures. Our IMACS f/2 observations occurred between 2011 July and 2011 October.

We also took advantage of the IMACS multi-object setup to conduct time-domain monitoring of three of our most densely populated fields. As described below in §4.6, our goal was to identify binary stars from radial velocity variations. We observed about 9 epochs of these fields, with baselines in time ranging from < 24 hours to days, weeks, months, and years. Since these fields overlap in area, a few stars were observed with up to twice as many observations.

Initial reduction of RIOTS4 IMACS multi-slit observations was completed with the Carnegie Observatories System for MultiObject Spectroscopy (COSMOS) data reduction package⁸. COSMOS was custom designed for use with the IMACS instrument and 8-CCD array setup. With COSMOS, we performed bias subtraction, flat-fielding, wavelength calibration, and extraction of 2-D spectra following the standard COSMOS pipeline. For single-star spectra from MIKE and IMACS, we used standard IRAF⁹ procedures to do bias subtraction, flat fielding, and wavelength calibration. From the wavelength-calibrated 2-D spectra for both single star observations and multi-slit observations, we used the *apextract* package in IRAF to find, trace, and extract 1-D spectra. We rectified the spectra using the *continuum* procedure and eliminated remaining cosmic rays or bad pixel values with the *lineclean* procedure, both of which belong to the *onedspec* package in IRAF.

3. RIOTS4 DATA PRODUCTS

3.1. Catalog of Spectral Types

The first observational data product from RIOTS4 is the catalog of spectral classifications for candidate field OB stars. The completeness of RIOTS4 allows a full characterization of the distribution of stellar spectral types in the field. We classify the stars based primarily on the atlas of OB spectra published by Walborn & Fitzpatrick (1990), and we also rely on Walborn et al. (2009) and Sota et al. (2011), especially for identification of unique spectral features. However, these atlases present mostly Galactic stars at solar metallicity ($Z \sim 0.02$), which is much higher than the SMC's

⁸ COSMOS was written by A. Oemler, K. Clardy, D. Kelson, G. Walth, and E. Villanueva. See <http://code.obs.carnegiescience.edu/cosmos>.

⁹ IRAF is distributed by the National Optical Astronomy Observatory, which is operated by the Association of Universities for Research in Astronomy (AURA), Inc., under cooperative agreement with the National Science Foundation (NSF).

metallicity ($Z \sim 0.004$). To investigate and eliminate potential biases in spectral types due to metallicity effects, we also refer to Walborn et al. (1995) and Walborn et al. (2000) for their comparison of stellar spectral types at Galactic and SMC metallicity. To obtain spectral types of supergiant stars, we adopt the criteria established by Lennon (1997) for SMC metallicity.

For an initial estimate, four of us (J. B. L., M. S. O., A. S. G., and J. B. G. M.) each independently estimated the spectral type of every star in the RIOTS4 survey using the above resources. We collated these spectral types and arrived at a consensus for each object. We finalized our catalog by plotting spectra sequentially from earliest to latest spectral types and iteratively maneuver stars within this sequence until we achieve a smooth transition between each spectral sub-type according to diagnostic stellar absorption line ratios. The majority of our spectra are accurate to within half a spectral type, so that, for example, an O8 star can reasonably be expected to have a spectral type between O7.5 and O8.5. However, for fainter objects and especially for spectral types later than B0 V, we sometimes list a range in their spectral types due to the faintness or non-detection of metal lines caused by a combination of poor S/N and the low metallicity of the SMC. Additional difficulties in spectral typing arise due to confusion from binary systems or Oe/Be stars, which have emission in one or more Balmer or He lines due to the presence of a circumstellar disk. These issues are discussed in more detail below.

We plot a sequence of RIOTS4 spectra in Figures 1 – 2, which cover spectral types from our earliest object, an O4 V star, to one of our latest objects, a B1.5 V star. For O stars, the diagnostic absorption line ratios are He II $\lambda 4542$ to He I $\lambda 4471$ and, as a secondary check, He II $\lambda 4200$ to He I(II) $\lambda 4026$. For B stars, the primary diagnostic absorption line ratio is Si IV $\lambda 4089$ to Si III $\lambda 4555$. A further constraint for early B type stars is the presence of He II $\lambda 4686$, which disappears at spectral types later than B0.2 V, B0.5 III, and B1 I.

We determine luminosity classes using a combination of spectral data as the primary diagnostic, and photometric magnitudes as a secondary check. To identify evolved stars at spectral types earlier than \sim O8, we look for the presence of emission features such as N II $\lambda\lambda 4634$ – 4640 – 4042 and weak absorption to strong emission in He II $\lambda 4686$. For later O stars, we use the increasing ratio of Si IV $\lambda 4089$ to He I $\lambda 4026$, which identifies increasingly evolved stars. In a similar manner, evolution in B stars is found in the increasing ratio of Si III $\lambda 4555$ to He I $\lambda 4471$. These luminosity effects are all demonstrated in the sample of evolved spectra shown in Figure 3. As mentioned previously, the lower metallicity of the SMC causes our spectra to have absent, or much weaker, metal lines than the Galactic spectral type standards in Walborn & Fitzpatrick (1990). In practice, the metal absorption lines tend to be absent in dwarf O stars for our observational setup, with the exception of C III $\lambda 4650$ in O9 – O9.5 V stars, but they do appear in giant or supergiant luminosity classes. We use the spectral criteria for SMC supergiants in Lennon (1997) to finalize our spectral types and luminosity classes for evolved stars.

For a final check on the luminosity class, we compare the expected magnitude of our established spectral type (Schmidt-Kaler 1982) at the distance of the SMC (DM

= 18.9; Harries et al. 2003) with the observed magnitude from Massey (2002). If the star is much brighter than expected for its luminosity class, then we re-visit our luminosity classification and adjust it to a more evolved class in more ambiguous cases. However, the existence of a binary companion would also increase the observed brightness of an object. Therefore, we carefully re-examine such stars for evidence of spectroscopic binary companions. Even so, detection of a secondary may often go unnoticed without multi-epoch observations, or they may be unresolvable due to low inclination angle, small mass ratio, or long periods. Thus, undetected binaries may be expected to bias our results slightly towards later spectral types and more evolved objects. In general, there is a tendency that the magnitudes indicate brighter luminosity classes than derived spectroscopically; this is related to the known effect that SMC OB stars are observed to lie above theoretical evolutionary tracks on the H-R diagram, as discussed by, e.g., Lamb et al. (2013) and Massey (2002). However, for Be stars, we find more extreme discrepancies in luminosity class, and we therefore omit these from the spectral classifications of Be stars in our catalog.

The fraction of our objects that are undetected binaries is likely to be significant; we obtain a lower limit to the binary fraction of $\sim 60\%$ in the RIOTS4 multi-epoch campaign (see §4.6), which is similar to the frequency found in open clusters (e.g., Sana et al. 2008, 2009, 2011). Thus, we want to quantify the potential effects undetected binaries will have on our spectral catalog. Furthermore, we require a method to determine spectral types of identified double-lined spectroscopic binaries. To address both these concerns, we create a sequence of synthetic binary stars, which we derive directly from the RIOTS4 spectral data. We begin by placing RIOTS4 stars with identical spectral classifications into separate groups. Any stars that have chip gaps affecting important diagnostic lines or have poor S/N are removed from these groups. The remaining stars in each group are wavelength-shifted to a radial velocity of zero and then median combined to create a template spectrum for each spectral type. We ensure that each template is created from a combination of at least five stars, which limits us to spectral types ranging from O8 to B1. Using these template spectra, we combine each pair, weighted according to their expected magnitudes (Schmidt-Kaler 1982), to generate our synthetic binary spectra. We plot an example sequence of these synthetic binaries in Figure 4. From this exercise, we find that the primary star in the system is rarely altered by more than a single spectral type. However, we find that the secondary spectral type is poorly constrained. This is especially true for O+B binaries, where the diagnostic Si III $\lambda 4555$ line for the B star, which is already weakened due to the low metallicity, is further affected by the continuum of the primary O star. Most binary systems with a B dwarf secondary star are undetectable in RIOTS4 spectra due to the weak Si III lines.

Another stellar population that creates issues for spectral typing is emission-line stars. In RIOTS4, this includes classical Oe/Be stars, supergiant B[e] (sgB[e]) stars (Graus et al. 2012), and Wolf-Rayet (WR) stars. These stars are often partially or wholly enshrouded in circumstellar disks or envelopes whose emission is su-

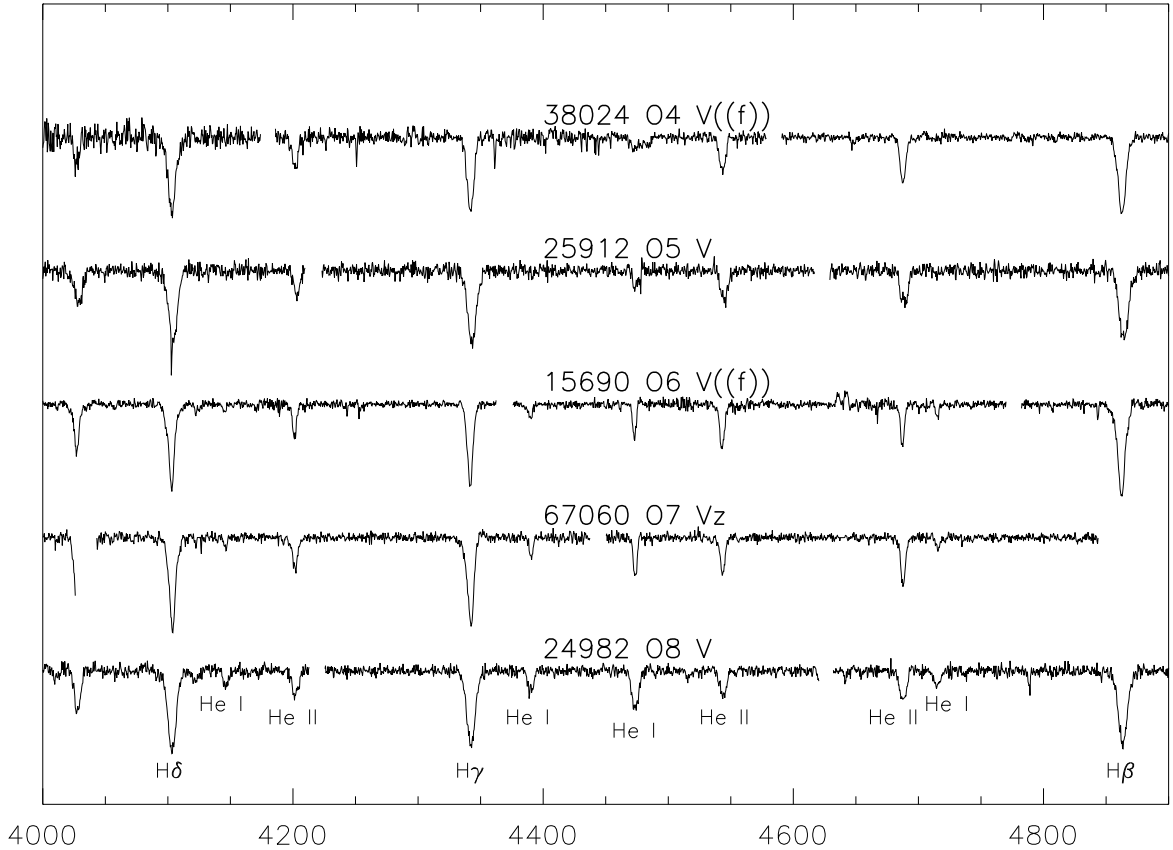


Figure 1. A sequence of spectral types from O4 V to O8 V stars from the RIOTS4 survey. We label the major spectral features in the range from 4000 – 4900 Å. The ratio of He II $\lambda 4542$ to He I $\lambda 4471$ is a primary spectral type diagnostic for O stars.

perimposed on the photospheric spectra. This results in weakened or absent absorption lines, which can drastically alter spectral types or make them impossible to determine. Lesh (1968) classifications for Oe/Be stars were carried out by JBG. In §4.7, we summarize our analysis of the four sgB[e] stars from Graus et al. (2012) and present the two WR stars, which are already known in the literature. While the number of sgB[e] stars and WR stars in our sample is small, classical Oe/Be stars account for 42% of the RIOTS4 sample (§4.7). Infill of the photospheric absorption lines often affects He I lines in Oe stars (e.g., Negueruela et al. 2004), and Si III $\lambda 4555$ and Si IV $\lambda 4089$ in Be stars. Golden-Marx et al. (2015) describe in more detail our approach to correcting for this effect in Oe stars.

Some stars in the RIOTS4 survey are included in previous spectroscopic studies of the SMC, including the limited study of field stars in the Magellanic Clouds by Massey et al. (1995) and the 2dF survey of the SMC by Evans et al. (2004). Our survey has a typical S/N ~ 75 and $R \sim 3000$, compared to S/N ~ 75 and $R \sim 1500$ for Massey et al. (1995), and S/N ~ 45 and $R \sim 1600$ for Evans et al. (2004). A comparison of spectral types for stars in common with Massey et al. (1995) shows agreement to within half a spectral type, consistent with our internal uncertainty. The stars in common between

the RIOTS4 and 2dF surveys show similar agreement with spectral type. However, many stars that we classify as dwarfs in RIOTS4 are listed as giants in 2dF. This discrepancy is linked to the problematic relation between observations and theoretical models mentioned above, and appears to result from our different methods for determining luminosity classes. Evans et al. (2004) rely more heavily on stellar magnitude and the equivalent width of H γ to determine luminosity classes due to the relatively poor spectral resolution and S/N of their data. Coupling this with the expected high binary fraction and our careful treatment of binaries may explain the differences.

3.2. Stellar Radial Velocities and Multi-Epoch Observations

Another important RIOTS4 data product is the measurement and distribution of radial velocities for SMC field OB stars. Radial velocities are an important property of a stellar population, both for individual objects and as an ensemble. Since runaways are a well known component of the field population, in principle, we can identify many such objects using their radial velocities. For the field stars as a whole, the velocity distribution and dispersion probe the kinematics of this population and on a large scale, the bulk motions of the SMC. For

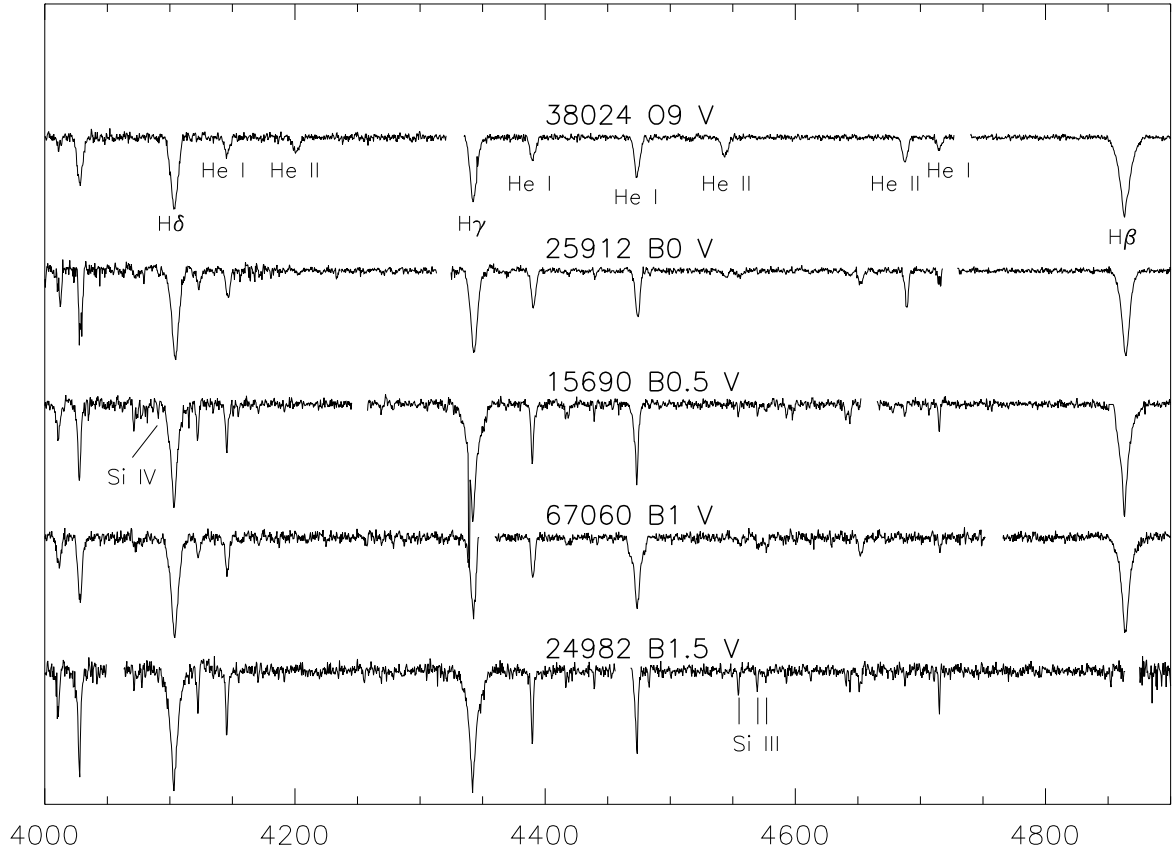


Figure 2. A sequence of spectral types from O9 V to B1.5 V from the RIOTS4 survey. We label the major spectral features in the range from 4000 – 4900 Å. With the transition from O to B type stars, the primary spectral diagnostic becomes the ratio of Si IV λ 4089 to Si III λ 4555, after He II disappears at spectral type B0.5 V.

multi-epoch observations, variability in the radial velocity is a strong indicator of a massive binary system.

We measure the radial velocities of RIOTS4 targets using the `rvidlines` package in IRAF. Velocities are obtained by fitting gaussian profiles to a combination of H, He I, and He II absorption lines. We require a minimum of 3 lines to determine the radial velocity, to ensure that continuum fitting issues or odd line profiles do not affect our measurements. Lines with velocities that significantly deviate from all other lines for a single star are excluded from the radial velocity measurement. These spurious velocities are typically associated with lines close to the IMACS chip gaps, which can affect the continuum fitting and, therefore, the line profile. The uncertainties on our radial velocity measurements are $\sim 5 \text{ km s}^{-1}$ for MIKE observations, $\sim 10 \text{ km s}^{-1}$ for IMACS f/4 observations, and $\sim 25 \text{ km s}^{-1}$ for IMACS f/2 observations.

Since massive stars have a high binary frequency, it is likely that a large fraction of our radial velocity measurements are affected by variability. Thus, single-epoch radial velocity measurements may cause erroneous identification of binary systems as runaway stars. This variability also adds scatter to the distribution of radial velocities for the full population. Our multi-epoch observa-

tions are meant to address the magnitude of these effects by measuring the scatter and estimating the field binary fraction for 8% of the RIOTS4 sample (§4.6). Our multi-epoch data are all obtained in IMACS f/4 mode, which gives us sensitivity to radial velocity variations of $\sim 10 \text{ km s}^{-1}$.

4. RESULTS

4.1. Stellar Catalog

Table 1 presents the basic catalog of the 374 objects in the RIOTS4 survey. In columns 1 – 3, we list the stellar ID numbers and B , V magnitudes from Massey (2002), respectively; column 4 contains the reddening-free Q_{UBR} calculated by Oey et al. (2004). In column 5, we provide an extinction estimate using the SMC extinction maps from Zaritsky et al. (2002). Column 6 contains the spectral classification derived from the RIOTS4 data. Columns 7 and 8 list our measured radial velocity of the star and the radial velocity of the nearest (in velocity space) H I kinematic component with brightness temperature $> 20 \text{ K}$ (see §4.5). We list the instrument setup used to obtain the spectrum in column 9 and the observation date in column 10. The Massey (2002) photometric errors are on average 0.01 at $V = 13.0$, and 0.04 at $V = 15.0$. Table 2 provides the same data for the

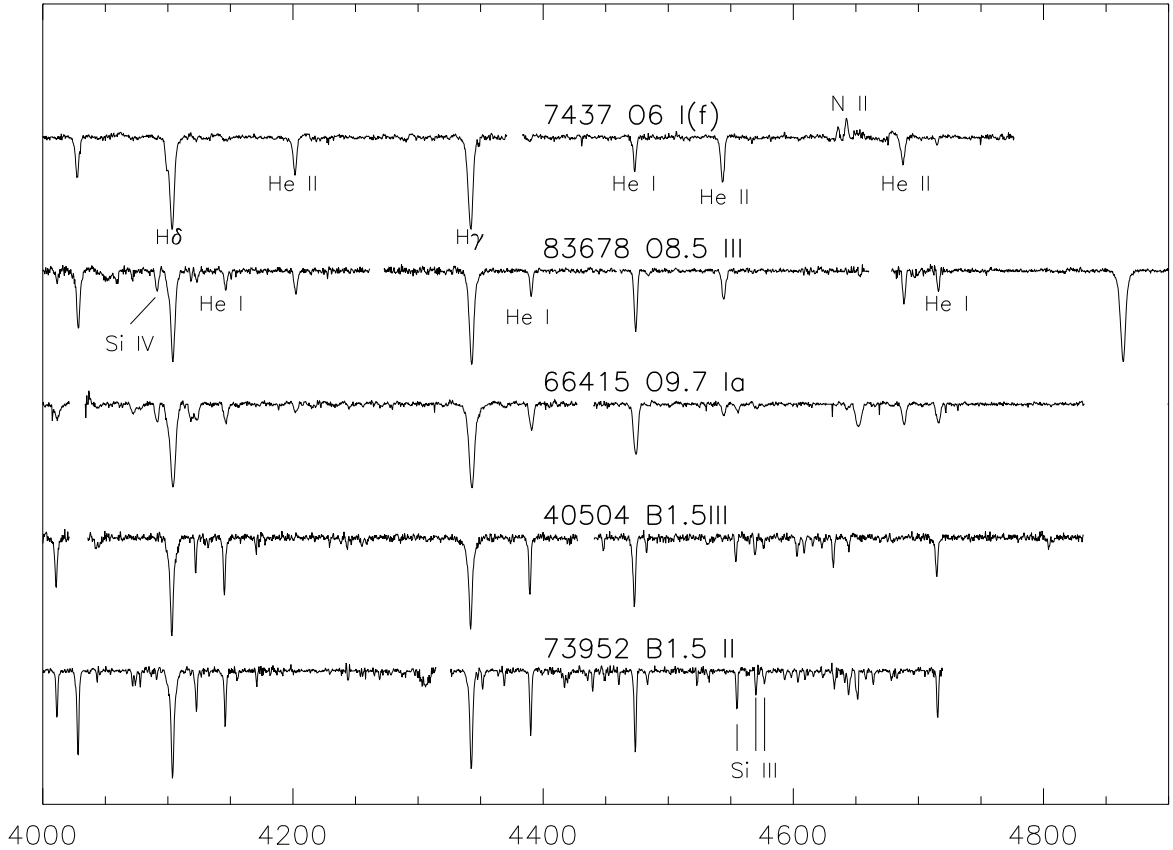


Figure 3. A sequence of evolved stars from O6 to B1.5 from the RIOTS4 survey. We label the major spectral features in the range from 4000 – 4900 Å. Except for the N II emission in the early O stars, evolved luminosity classes are primarily identified by the strength of the Si IV for late O stars and Si III for early B stars.

23 additional stars we observed from the UV-selected sample. In what follows, we consider only the original, optically selected sample so that our analysis is applied strictly to a uniformly selected sample. However, given that there are 23 additional stars out of 91 identified with the alternate criteria, we can infer that our base sample is incomplete at least at the 25% level for identifying all actual OB stars.

4.2. Field IMF

Previous studies of the field massive star IMF in the Magellanic Clouds indicate a slope steeper than the traditional Salpeter slope of $\Gamma = 1.35$. The observed slopes range from $\Gamma = 1.80 \pm 0.09$ (Parker et al. 1998) to $\Gamma \sim 4.0 \pm 0.4$ (Massey et al. 1995; Massey 2002). However, not all studies agree on this point, as observations of “field” stars in the LMC region surrounding 30 Dor suggest an IMF consistent with Salpeter (Selman et al. 2011). Some of the uncertainty and variation in these results can be attributed to obtaining the IMF using only photometry or a combination of photometry and spectroscopy. As shown by, e.g., Massey (2011), deriving accurate masses for massive stars can only be done with spectroscopy. If spectroscopically determined masses confirm the steep field IMF then it would repre-

sent the largest deviation from the traditional Salpeter IMF obtained from direct star counts. RIOTS4 was designed for such observations, since it avoids the uncertainty of photometric masses, and our large sample minimizes stochastic effects at the highest masses.

With RIOTS4, we definitively measure the field massive star IMF with our spatially complete sample of objects; full details on methodology and results are reported by Lamb et al. (2013). Briefly, for stars with spectroscopically derived masses $> 20 M_{\odot}$, we follow Koen (2006) to derive the cumulative mass distribution for the SMC field and compare it with evolved present-day mass functions from Monte Carlo models with ages up to 10 Myr, the lifetime of $20 M_{\odot}$ stars. Using this method, we estimate that the field massive star IMF slope is $\Gamma = 2.3 \pm 0.4$ for the the highest-mass SMC stars. This slope is confirmed with OGLE II photometry (Udalski et al. 1998) for $7 - 20 M_{\odot}$ stars, using a stochastic approach that models the uncertainties in stellar positions on the H-R diagram. With further Monte Carlo modeling, we determine that undetected binaries or a unique star formation history are unable to explain this steep field IMF. Thus, we conclude that the steep observed IMF is a real property of the SMC field. In §5, we attribute this to a preponderance of tiny star-forming

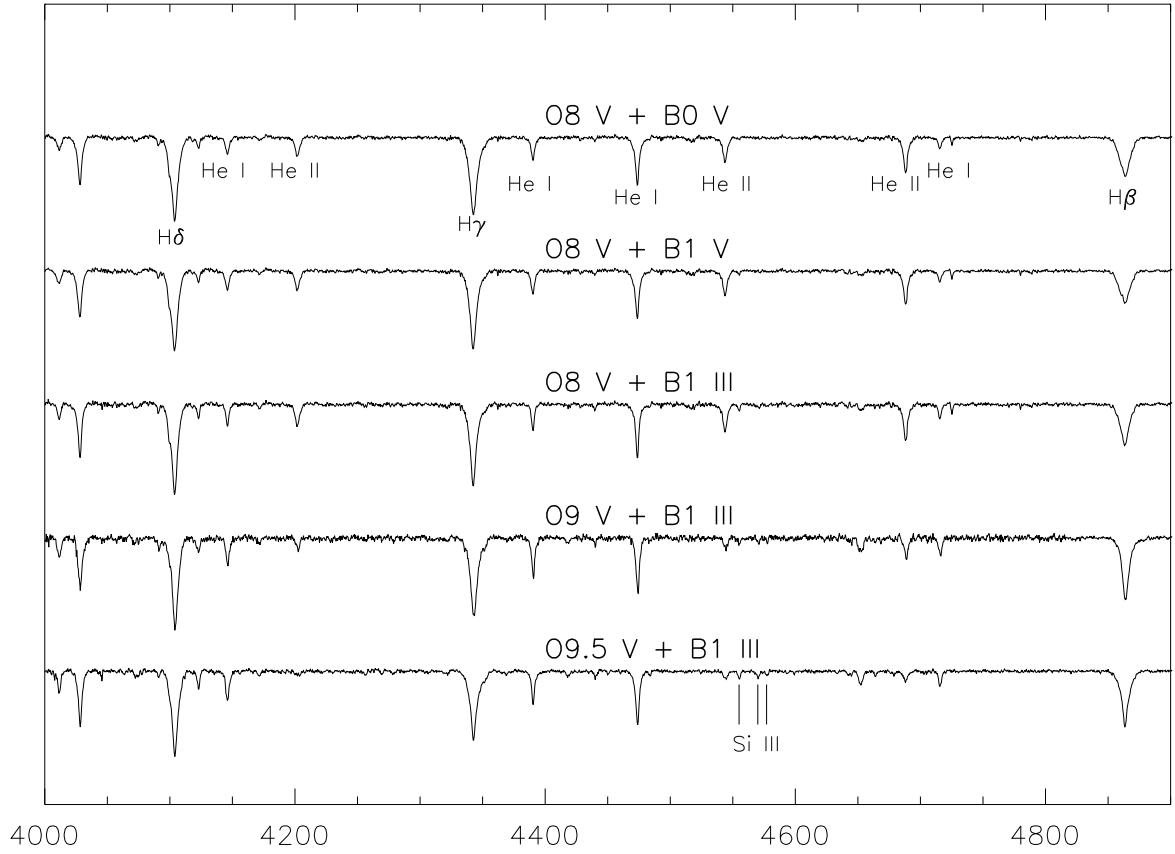


Figure 4. A sample of synthetic binary spectra derived from actual RIOTS4 spectra. We label the major spectral features in the range from 4000 – 4900 Å. The top pair of spectra demonstrate the difficulty of identifying spectroscopic binaries that consist of an O star and a dwarf B star, due to the weakness of the Si III lines. However, the likely undetected companion does change the apparent spectral type of the spectrum from O8 to O8.5. In contrast, the bottom three spectra demonstrate the ease with which a primary O star can be identified with a giant B star companion, due to the clear presence of both He II and Si III.

Table 1
RIOTS4 Catalog^a

ID ^b	B^b	V^b	Q_{UBR}	A_V^c	Sp Type	RV_{star} (km s ⁻¹)	RV_{HI}^d (km s ⁻¹)	Instrument	Observation Date (YYMMDD)
107	14.96	15.00	-0.95	0.82	Be ₃	–	–	MIKE	111024
298	15.18	15.12	-0.91	1.03	B1e ₃₊	–	–	IMACS f/4	070920
1037	15.15	15.28	-0.85	0.44	B0.5 V	110	110	IMACS f/4	070920
1600	14.42	14.60	-0.87	0.32	O8.5 V	93	103	IMACS f/4	070920
1631	15.19	15.15	-0.99	1.11	B1e ₂	120	120	IMACS f/4	070920

^a This table is published in its entirety in the electronic edition of the *Astrophysical Journal*. A portion is shown here for guidance regarding its form and content.

^b From Massey (2002).

^c From Zaritsky et al. (2002).

^d Measured from Stanimirović et al. (1999).

Table 2
Additional UV-Optically Selected Stars in the SMC Bar

ID ^a	B^a	V^a	Q_{UBR}	A_V^b	Sp Type	RV_{star} (km s ⁻¹)	RV_{HI}^c (km s ⁻¹)	Instrument	Observation Date (YYMMDD)
5391	13.36	13.31	-1.00	1.13	O8.5 III	44	98	IMACS f/4	060913 ^d
6946	14.60	14.69	-0.87	0.57	O9.5 V	141	141	IMACS f/4	060913 ^d
8257	14.69	14.49	-0.87	1.55	B1.5 V	96	107	IMACS f/4	060913 ^d
9534	13.63	13.76	-0.84	0.44	B0.2 III	-	-	IMACS f/4	090824
10129	13.87	14.01	-0.87	0.45	B0.2 V	130	130	IMACS f/4	060913 ^d
14190	15.04	14.83	-0.99	1.46	B1.5 V	149	149	IMACS f/4	090824
15203	14.06	14.11	-0.87	0.69	O9.5 V + O9.7 V	156	156	IMACS f/4	060912
15440	14.97	14.77	-0.90	1.49	B1e ₃	-	-	IMACS f/4	090825
15690	14.05	14.07	-0.99	0.89	O6 V((f))	80	120	IMACS f/4	090824
17963	15.12	15.21	-0.99	0.55	B0.2 V	115	120	IMACS f/4	090824
18200	14.33	14.33	-0.87	0.90	B0e ₃	111	120	IMACS f/4	090824
24982	14.75	14.94	-0.85	0.26	O8 V	110	110	IMACS f/4	060913 ^d
25912	14.19	14.39	-0.88	0.26	O5 V	150	150	IMACS f/4	060913 ^d
27272	13.62	13.78	-0.85	0.35	B0.7 III + B	121	121	IMACS f/4	060913 ^d
28153	14.69	14.83	-0.88	0.41	O9.5 V	169	169	IMACS f/4	060912
36359	14.38	14.30	-1.03	1.25	B1e ₄₊	-	-	IMACS f/4	060912
38302	14.64	14.81	-0.84	0.29	B1 V	154	154	IMACS f/4	090825
40341	13.77	13.98	-0.92	0.24	O8.5 III((f))	-	-	IMACS f/4	090825
41095	14.84	14.85	-0.92	0.92	O9.5-B0 V + Be ₃	-	-	IMACS f/4	060911
44634	15.19	15.37	-0.85	0.27	O9.5-B0 V	150	150	IMACS f/4	090825
45677	13.52	13.66	-0.92	0.47	O9.5 III	160	164	IMACS f/4	090825
48672	14.34	14.52	-0.93	0.36	O7.5 V	-	-	IMACS f/4	090824
53373	14.08	14.20	-0.84	0.51	O9 V	119	122	IMACS f/4	090824

^a From Massey (2002).

^b From Zaritsky et al. (2002).

^c Measured from Stanimirović et al. (1999).

^d Observed multiple times for binary monitoring; see Table 3.

events.

4.3. *In Situ Formation of Field O Stars*

As outlined earlier, the origin of the field massive star population is an open question. In particular, it is unknown whether massive stars are capable of forming in isolation or within sparse clusters. Some theories of massive star formation, such as competitive accretion, suggest that the most massive star formed in a cluster depends on the cluster mass (Bonnell et al. 2004). Other theories, such as those based on core accretion, allow for the formation of massive stars in sparse environments, or even in isolation (e.g., Krumholz et al. 2009). The essential question is whether the formation of massive stars in sparse environments is merely improbable (e.g., Elmegreen 2000) or actually impossible (e.g., Weidner & Kroupa 2006).

Using RIOTS4 spectra, along with data from the *Hubble Space Telescope* (*HST*) (Lamb et al. 2010) and OGLE photometry (Udalski et al. 1998), we identify a sample of unusually strong candidates for in-situ, field OB star formation. Lamb et al. (2010) discover three massive stars that formed in sparse clusters containing ~ 10 or fewer companion stars with mass $> 1M_{\odot}$ and another three candidates for truly isolated formation. Oey et al. (2013) present a sample of 14 field OB stars that are centered on symmetric, dense H II regions, which minimizes the likelihood that these objects have transverse runaway velocities. In both studies, the RIOTS4 spectra eliminate line-of-sight runaways, leaving strong candidates for field massive stars that formed in situ. We set further constraints on the degree to which these stars are isolated by examining their immediate stellar environments with the *HST* and OGLE imaging, allowing us to evaluate the relationship between the most massive stars in any sparse clusters and the cluster mass. Our results imply that these two quantities are independent, and thus they favor the core collapse models for massive star formation.

4.4. *Radial Velocity Distribution*

The distribution of radial velocities reveals information about the stellar population kinematics, as well as the bulk motion of the SMC. Our velocity distribution from RIOTS4 is generally consistent with earlier work; Figure 5 is qualitatively similar to that found from the 2dF survey of OBA-type stars in the SMC found by Evans & Howarth (2008). Both samples exhibit a gaussian-like velocity distribution with a FWHM of ~ 30 km s $^{-1}$ and a mean systemic velocity of ~ 150 km s $^{-1}$. As mentioned earlier, radial velocities for individual stars may be affected by binary motions, and so we can only make inferences based on aggregate trends. We do see evidence of a velocity gradient across the SMC, which we depict in Figure 6 by plotting velocity distributions of three regions in the SMC. The Bar 1 and Bar 2 regions have mean velocities of 140 km s $^{-1}$ and 157 km s $^{-1}$, respectively, with corresponding respective velocity dispersions of 32 km s $^{-1}$ and 39 km s $^{-1}$. Note that although we bisect the bar into two regions, it appears to have a relatively smooth velocity gradient. The SMC wing is more redshifted than the SMC bar, having a mean velocity of 177 km s $^{-1}$ with velocity dispersion of 29 km

s $^{-1}$, but it does not appear to have a significant internal velocity gradient. These observations of the large-scale motions in the SMC agree with results based on stars in the 2dF survey and on H I gas from Stanimirović et al. (2004).

4.5. *Runaway Stars*

Runaway stars are a well-known component of the field population, yet their relative contribution to the field and ejection mechanisms from clusters remain poorly understood. Observational estimates for the runaway frequency range from 10% (Blaauw 1961) to 50% (de Wit et al. 2005), while some authors argue that *all* field massive stars are runaways (Gvaramadze et al. 2012). One trend that seems to have emerged is that O stars have a 2 – 8 times higher runaway frequency than B stars (e.g., Gies 1987; Stone 1991). Runaways arise from one of two likely methods: the binary supernova scenario (Blaauw 1961), or the dynamical ejection scenario (Poveda et al. 1967). In the binary supernova scenario, the primary star in a massive binary explodes as a supernova, which drops the gravitational binding energy of the system and may impart a kick to the secondary star. In contrast, dynamical ejections primarily arise from three- or four-body interactions between a massive binary and single star or massive binary pairs (e.g., Leonard & Duncan 1990). These ejection mechanisms will imprint different quantitative properties on the runaway population, including velocities, binary parameters, and chemical composition. For example, the binary supernova scenario cannot produce runaway velocities above ~ 200 km s $^{-1}$, while dynamical ejections can attain higher velocities (Gvaramadze et al. 2009, and references therein). Both ejection scenarios are predicted to include binary runaways; however, the type of binaries differ significantly. For the binary supernova scenario, the compact object remnant of the primary star sometimes remains bound to the secondary as a runaway binary system with an eccentric orbit (McSwain et al. 2007). For dynamical ejections, tight binaries are sometimes ejected as a single system, thus representing the only mechanism that can form a runaway double-lined spectroscopic binary. Finally, while both mechanisms originate from binary systems, stars ejected from the binary supernova scenario may be He-rich due to contamination from the supernova explosion (Hoogerwerf et al. 2001).

To estimate the fraction of runaway stars in the RIOTS4 sample, we compare the observed stellar radial velocities of our OB stars with the H I gas velocity distribution along the line of sight, using data from the Australia Telescope Compact Array (ATCA) and Parkes telescopes compiled and mapped by Stanimirović et al. (1999). We identify runaway candidates as those objects with radial velocities that are different by > 30 km s $^{-1}$ from those of the nearest H I velocity components having a brightness temperature > 20 K in the same line of sight. A pair of examples are shown in Figure 7, with star 35491 depicting an object consistent with the line-of-sight H I gas velocity, and star 43724 meeting our criteria for a runaway star. We find that only 11% of the stars meet these runaway criteria, 27 out of 238 stars with good radial velocity determinations. This frequency is likely to be overestimated due to false positives caused by binary

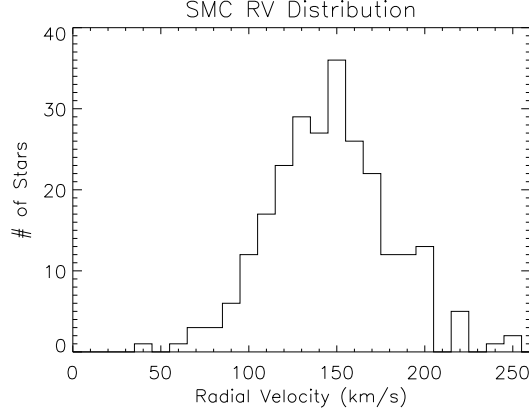


Figure 5. The distribution of radial velocities from stars in the RIOTS4 survey.

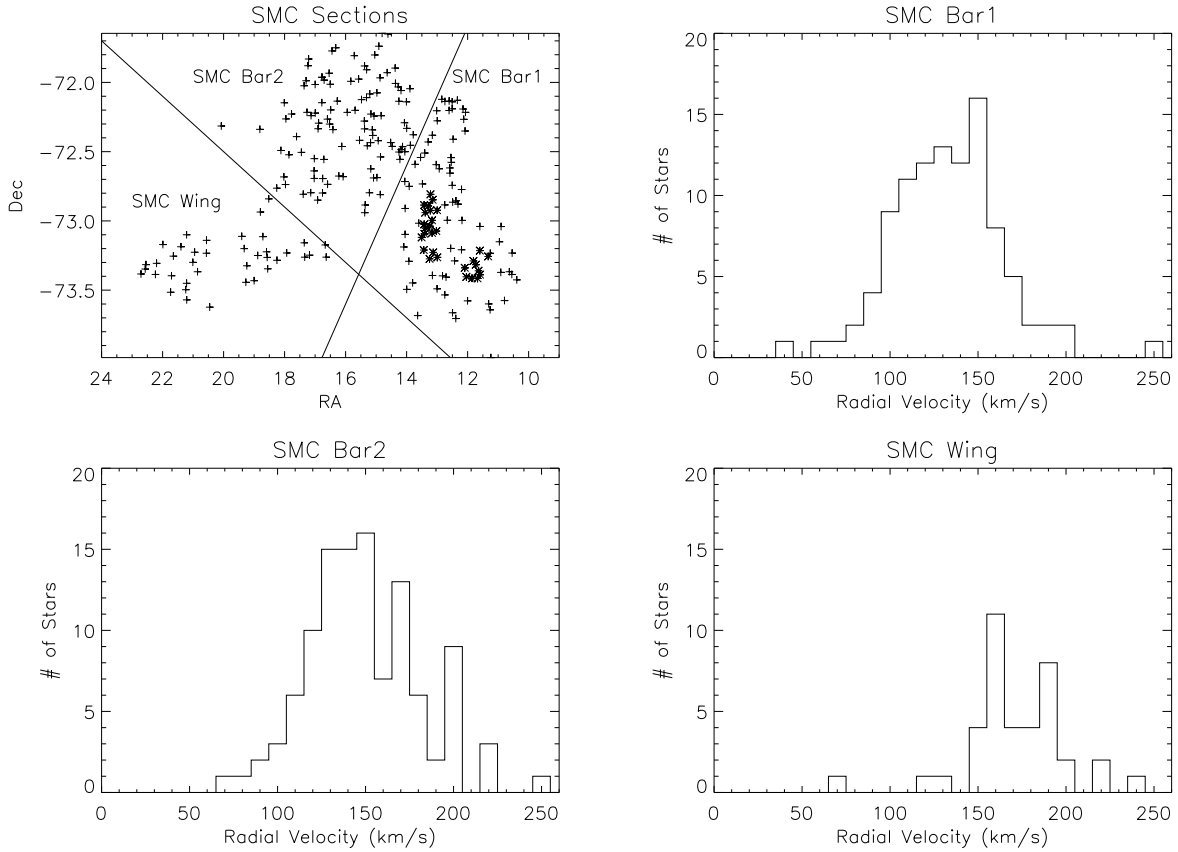


Figure 6. We split the RIOTS4 sample into three regions of the SMC, as shown in the upper left panel. Stars in our binary fields are plotted with asterisks while all other stars are plotted as crosses. In the other three panels, we plot the radial velocity distribution for stars in each separate region. The clear velocity gradient of RIOTS4 stars across the SMC agrees qualitatively with the velocity gradient of HI gas from Stanimirović et al. (2004).

motions, since the measured radial velocity may reflect the orbital motion for a binary star, rather than the systemic velocity. While such motions will also sometimes cause false negatives depending on the orbital configuration at the time of observation, false positives are more likely to be observed. A more significant effect is that radial velocities can only identify line-of-sight runaway motions. We estimate that our observations miss 50% of runaways if the typical ejection velocity is ~ 60 km

s^{-1} . Since only 8% of our survey has multi-epoch observations, we are not yet able to correct for the effect of binaries on the stellar population kinematics. Therefore, we have initiated further follow-up, binary monitoring observations to further minimize these degeneracies.

We do find one runaway, star 5391, that we identify as a binary star from our multi-epoch observations (§ 4.6). Its radial velocity of 44 km s^{-1} is 55 km s^{-1} removed from the nearest significant component of HI gas. With

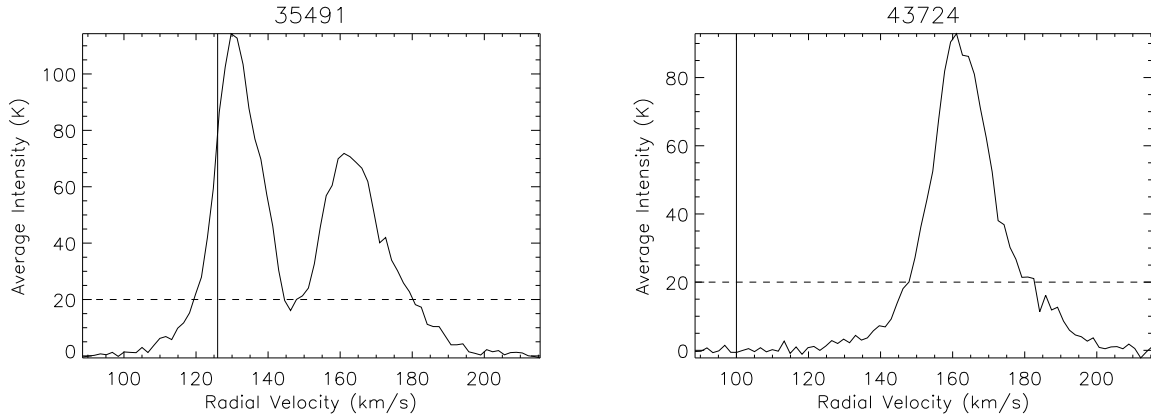


Figure 7. Position-velocity diagrams for H I in the line of sight for two RIOTS4 stars, showing data from Stanimirović et al. (2004). The solid, vertical line depicts the observed radial velocity of the RIOTS4 target, while the dashed line shows our brightness temperature threshold of 20 K. Stars 35491 (left) and 43724 (right) are examples for which the stellar and gas velocities are consistent and inconsistent, respectively.

a semi-amplitude of 108 km s^{-1} in our observed variations, the secondary cannot be a degenerate star. Therefore, if this binary system is indeed ejected from a cluster, then it must be due to the dynamical ejection mechanism rather than the binary supernova mechanism. Since dynamical ejection frequently splits binaries, the existence of a non-degenerate, runaway binary suggests a major contribution by this process to the runaway population.

Another interesting object also points to the importance of dynamical ejection: Star 49937 appears to be an extreme runaway that is unlikely to be the product of the binary supernova scenario. Its runaway velocity is $\sim 200 \text{ km s}^{-1}$ removed from the nearest H I velocity component. While it is possible that this star’s runaway component is completely in the line of sight and/or fortuitously enhanced by binary motion, its high radial velocity, taken at face value, is near the maximum ejection speed possible from the binary supernova mechanism (Portegies Zwart 2000), as mentioned above. Thus, the existence of this star again suggests a significant role for dynamical ejection of runaways.

4.6. Binary Stars

Stellar multiplicity is a key parameter that probes the formation and dynamical evolution of a stellar population. For example, large protostellar disks may be disrupted in high-density environments, thereby suppressing the formation of massive binaries (Kratter et al. 2008, 2010). Recent studies of Galactic clusters and OB associations find observed massive-star binary fractions ranging from $\sim 60\%$ to $\sim 80\%$ (e.g., Sana et al. 2008, 2009, 2011; Kiminki & Kobulnicky 2012; Kobulnicky et al. 2014). However, few studies have systematically investigated the multiplicity of massive stars in the field. Early studies found that field massive stars have roughly half the binary frequency of massive stars found in clusters (e.g., Stone 1981; Gies 1987). This general trend of a lower field binary frequency persists in later studies, such as Mason et al. (1998, 2009), who use speckle interferometry of objects in the Galactic O Star Catalog (Maíz-Apellániz et al. 2004) to compare the frequency of multiplicity between cluster and field O stars. In this magnitude-limited sample, they find a 39% bi-

nary fraction for field O stars, compared to a 66% binary fraction for O stars in clusters. When combining their results with data from the literature on spectroscopically identified binaries, they obtain 51% and 75% binary fractions for field and cluster O stars, respectively. However, the spectroscopic data for these objects is non-uniform and therefore may not provide an accurate comparison of these statistics between cluster and field O stars. But it does suggest that the frequency of multiplicity for massive stars in the Galactic field is lower than in clusters.

With the RIOTS4 survey, we performed repeat observations of three IMACS slit-mask fields over the 5-year survey period, totaling 29 objects, to obtain an initial evaluation of the binary fraction of field massive stars in the SMC. We note that some of these stars belong to the UV-selected sample (Table 2), rather than the default sample. We have 9 – 10 epochs for each field, at intervals of days, weeks, months, and years apart; three stars appear in two of the three fields, yielding up to twice the number of observations for these objects. As with the larger survey, these fields have a high fraction of Oe/Be stars, and we focus here primarily on the 17 non-Oe/Be stars in these fields. We use three separate methods to identify potential binaries, which are described below. The first method identifies binaries using maximum observed radial velocity variations, the second method is based on a statistical F-test analysis following Duquenois & Mayor (1991), and the third method uses the period power spectrum and searches for binary orbital solutions from the radial velocity data. Table 3 summarizes this binary monitoring sample: columns 1 and 2 give the star ID and spectral type, respectively; column 3 gives the number of observations, and columns 4 and 5 show the star’s binary status determined from the second and third methods; we note that the first method yields the same results as the second. Column 6 gives the systemic velocity based on the orbital solution, if available, or the mean of the minimum and maximum measured radial velocities. Column 7 gives the largest velocity variation observed within a 14-day interval Δv , and column 8 provides the standard deviation σ_{obs} of the radial velocity measurements for each star. Column 9 lists the calculated $P(\chi^2)$, which is used to determine

binary status in the statistical F-test (§4.6.2). Column 10 shows the observation dates for each object, coded as indicated.

4.6.1. Maximum radial velocity variation and timescale

To identify binary star candidates, we first compare the amplitude of radial velocity variations with the timescale of the variations. Since the amplitude of radial velocity variations is inversely correlated with the period of a binary system, binaries with large-amplitude variation should display variability on short timescales, provided the eccentricity of the system is near zero. In Figure 8, we plot the amplitude of the maximum observed radial velocity variation over short timescales (< 14 days; Table 3) versus the amplitude of the maximum radial velocity variation over any time scale. Note that in Figure 8 all objects must lie at or below the dashed identity line. In an ideal scenario, all short-period systems will lie along this locus; however, we cannot expect good sampling with $\lesssim 10$ epochs of data. Nonetheless, we still observe a large fraction of high-variation systems along the identity line, which suggests there are no systematic velocity offsets over time. Given the sampling of these fields and our systematic errors, we conservatively identify binaries as those objects with radial velocity variations $> 30 \text{ km s}^{-1}$ including errors. This yields 10 probable binaries out of the 17 non-Oe/Be stars in our binary monitoring fields.

4.6.2. F-test: radial velocity variations relative to noise

We also use the approach of Duquennoy & Mayor (1991) who identified binary candidates in the nearby solar neighborhood. This method compares the mean of the statistical measurement errors associated with each radial velocity measurement (σ_{ave}) with the standard deviation in the measured radial velocities (σ_{obs} ; Table 3) for each star. For single objects with properly estimated measurement errors, the ratio of $\sigma_{\text{obs}}/\sigma_{\text{ave}}$ should be approximately equal unity. However, it is unclear where the cutoff ratio between single objects and binary stars should occur. Thus, Duquennoy & Mayor (1991) use a statistical F-test to measure the probability $P(\chi^2)$ that the observed variations are due to statistical noise. Following their work, we calculate χ^2 , accounting for the number of observations n , with:

$$\chi^2 = (n-1)(\sigma_{\text{obs}}/\sigma_{\text{ave}})^2 \quad . \quad (2)$$

Using the cumulative chi-square distribution given by

$$F_k(\chi^2) = G(k/2, \chi^2/2) \quad (3)$$

where G is the regularized Gamma function for a given degree of freedom $k = n - 1$, we calculate $P(\chi^2) = 1 - F_k(\chi^2)$, given in Table 3. In the case that all objects are single, the distribution of $P(\chi^2)$ should be uniform between values of 0 and 1. Binary systems, on the other hand, should have very low values of $P(\chi^2)$, since their radial velocity variations are not due to statistical noise. Thus, we can identify binaries as those objects with $P(\chi^2) < 0.01$. We plot the distribution of $P(\chi^2)$ for the same 17 stars in Figure 9. Again, we find a high binary fraction with 10 out of 17 objects having $P(\chi^2) < 0.01$.

4.6.3. Period power spectrum

We used the radial velocities to search for credible orbital solutions for all the stars in the binary monitoring sample based on the method described by Kiminki et al. (2012). In this approach, we generate the power spectrum of periods for each object, and identify the most likely values, if any, with an IDL program created by A. W. Fullerton, which uses the CLEAN deconvolution algorithm of Roberts et al. (1987). We then apply the Gudehus (2001) code for determining orbital solutions, the Binary Star Combined Solution Package, using the candidate periods. We show the phase diagrams of the two best orbital solutions in Figure 10. These are for stars 10129 and 27600, with periods around 4.8 and 3.3 days, respectively. Star 10129 appears to have a moderate eccentricity around $e = 0.2$, while 27600 is consistent with a purely circular orbit. This approach again yields 10 out of 17 probable binaries, although the identified candidate binaries are not the exact same ones found with the preceding methods (Table 3).

4.6.4. Binary Fraction

All three binary identification methods suggest binarity in 10 out of 17 ($59\% \pm 12\%$) of the non-Oe/Be stars in our three binary monitoring fields. This frequency is consistent, within the uncertainty, with previous observations of multiplicity in the Galactic field, which are $\sim 40-50\%$ as described above. However, the small number statistics generate large errors, and our binary frequency is actually closer to values observed in Galactic clusters and OB associations. It is further difficult to compare these frequencies because of the different observational biases inherent in the different binary detection methods and sample properties; our frequencies are lower limits, representing results only for spectroscopic binaries. Sota et al. (2014) find a strong lower limit of 65% for the combined spectroscopic and visual binaries in the southern component of their Galactic O star survey. Almost one quarter of these are identified exclusively by astrometric methods. We have started follow-up monitoring of additional RIOTS4 targets to confirm these results, and to obtain binary orbital parameters.

We also applied the third binary identification method to the remaining 12 stars in the monitoring fields, which are classical Oe/Be stars. The radial velocities measured for these stars are more uncertain than for normal stars because of emission-line contamination in the H lines. We find that 6 out of the 12 Oe/Be stars appear to be probable binaries.

One of our binaries, star 27272, is a double-lined spectroscopic binary (SB2) with B0.7 III and B star components (Figure 11). In our observations of this system, we find that the stronger absorption line appears blueshifted in all but 1–2 epochs. While this may be evidence of the Struve-Sahade (S-S) effect (Struve 1937; Sahade 1959), it is most likely caused by an unfortunate observing cadence, which impedes our ability to obtain a satisfactory orbital solution.

4.6.5. Systemic Velocities

Estimated systemic velocities v_{sys} for the 29 stars in the monitoring fields are given in Table 3. These are generally given as the average of the minimum and maximum

Table 3
Stars in binary monitoring fields

ID	SpT	<i>N</i>	F-test	Power Spec	v_{sys} (km s ⁻¹)	Δv (km s ⁻¹)	σ_{obs} (km s ⁻¹)	$P(\chi^2)$	Observation Dates ^a
Normal OB Stars									
5391	O8.5 III	9	Y	Y	44	144	75	< 0.01	ABCEFGHIJK
6908	O9.5 – B0 III	9	Y	N	128	93	25	< 0.01	ABCEFGHIJK
6946	O9.5 V	9	N	N	141	35	12	0.74	ABCEFGHIJK
7437	O6.5 I(f)	9	Y	Y	151	29	33	< 0.01	ABCEFGHIJK
7782	O8 V	9	Y	Y	127	65	33	< 0.01	ABCEFGHIJK
8257	B1.5 V	9	Y	Y	96	61	21	< 0.01	ABCEFGHIJK
8609	B0 III	9	N	N	128	21	11	0.97	ABCEFGHIJK
10129	B0.2 V	9	Y	Y	130 ^b	29	21	< 0.01	ABCEFGHIJK
10671	B0.5 V	9	Y	N	122	108	33	< 0.01	ABCEFGHIJK
21844	O8 III((f))	9	N	N	151	36	13	0.09	BCDEFGHIJK
24213	B0 III	16	N	N	126	6	9	0.99	ABCDEFGHIIJK
24982	O8 V	8	Y	Y	110	59	32	< 0.01	ADFGHIJK
25912	O5 V	9	Y	Y	150	103	45	< 0.01	ADEFGHIJK
27272	B0.7 III + B	9	Y	Y	121 ^c	223	105	< 0.01	ADEFGHIJK
27600	B0.5 III	10	N	Y	177 ^b	16	13	0.64	BCDEFGHIJK
27712	B1.5 V	7	N	N	127	8	7	0.46	ADFGHIJK
28841	B1 III	10	N	Y	141	22	15	0.02	BCDEFGHIJK
Classical Oe/Be Stars									
7254	O9.5 IIIe ₂	9	...	Y	126	10	ABCEFGHIJK
21933	Be ₃	4	...	N	130	57	AHIJ
22321	O9.5 IIIpe ₄₊	10	...	Y	167 ^b	28	BCDEFGHIJK
23710	O9–B0 pe ₃₊	10	...	N	168	48	BCDEFGHIJK
23954	B1.5e ₃₊	7	...	N	130	69	ADFGHIJ
24229	B1e ₂	7	...	N	155	19	ADFGHIJK
24914	O9 III–Vpe ₁	4	...	Y	81	20	AEHI
25282	B0e ₁	17	...	N	130	72	ABCDEFGHIIJK
25337	Be ₃	9	...	Y	124	55	BCDEFGHIJK
27135	B1e ₂	18	...	N	113	30	BCDEFGHIJK
27736	B0e ₂	6	...	Y	153	39	DEFGHIJ
27884	O7–8.5 Vpe ₄₊	10	...	Y	156	32	BCDEFGHIJK

^a Dates of observation are coded as follows: (A) 2006 September 13, (B) 2007 September 19, (C) 2007 September 20, (D) 2008 September 24, (E) 2008 October 6, (F) 2008 October 7, (G) 2008 October 11, (H) 2008 November 21, (I) 2008 November 22, (J) 2009 August 24, (K) 2010 December 20.

^b From orbital solution.

^c Average of SB2 components A and B.

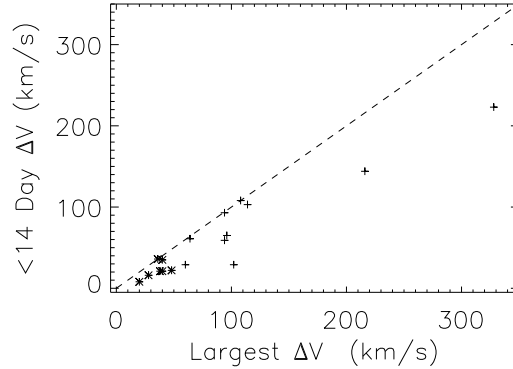


Figure 8. The observed maximum short-term (< 14 days) radial velocity difference vs the largest radial velocity difference over any period. The dashed line depicts the identity relationship. Objects with the highest observed velocity difference happening over a < 14 day period will lie on this line. We expect real binary systems will exhibit velocity variations on both long and short term periods. Binaries identified by having radial velocity variations > 30 km s⁻¹ are plotted with a plus sign, while single stars are depicted as asterisks.

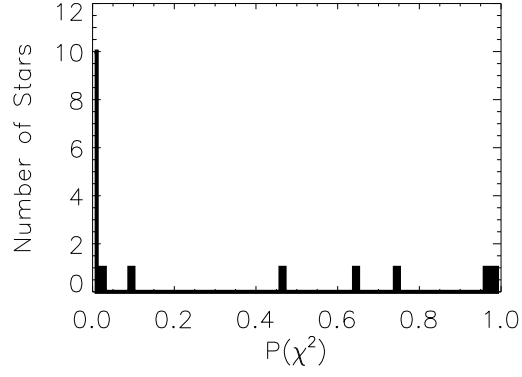


Figure 9. The distribution of $P(\chi^2)$ for non-Oe/Be stars in our binary fields. Binary systems that exhibit radial velocity variations significantly larger than expected from observational errors will have very low $P(\chi^2)$ values (< 0.01).

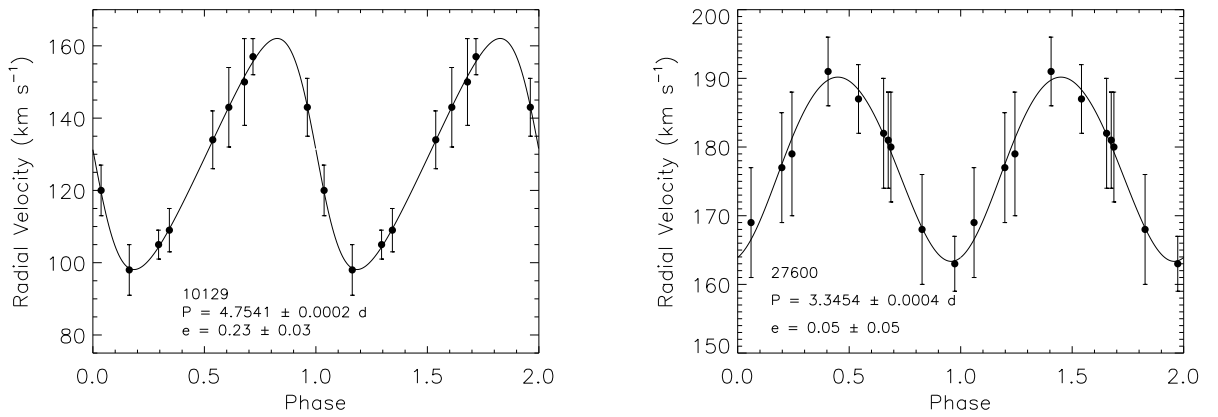


Figure 10. Phase diagrams showing the solutions for two more securely identified binaries among the normal OB stars in the monitoring sample.

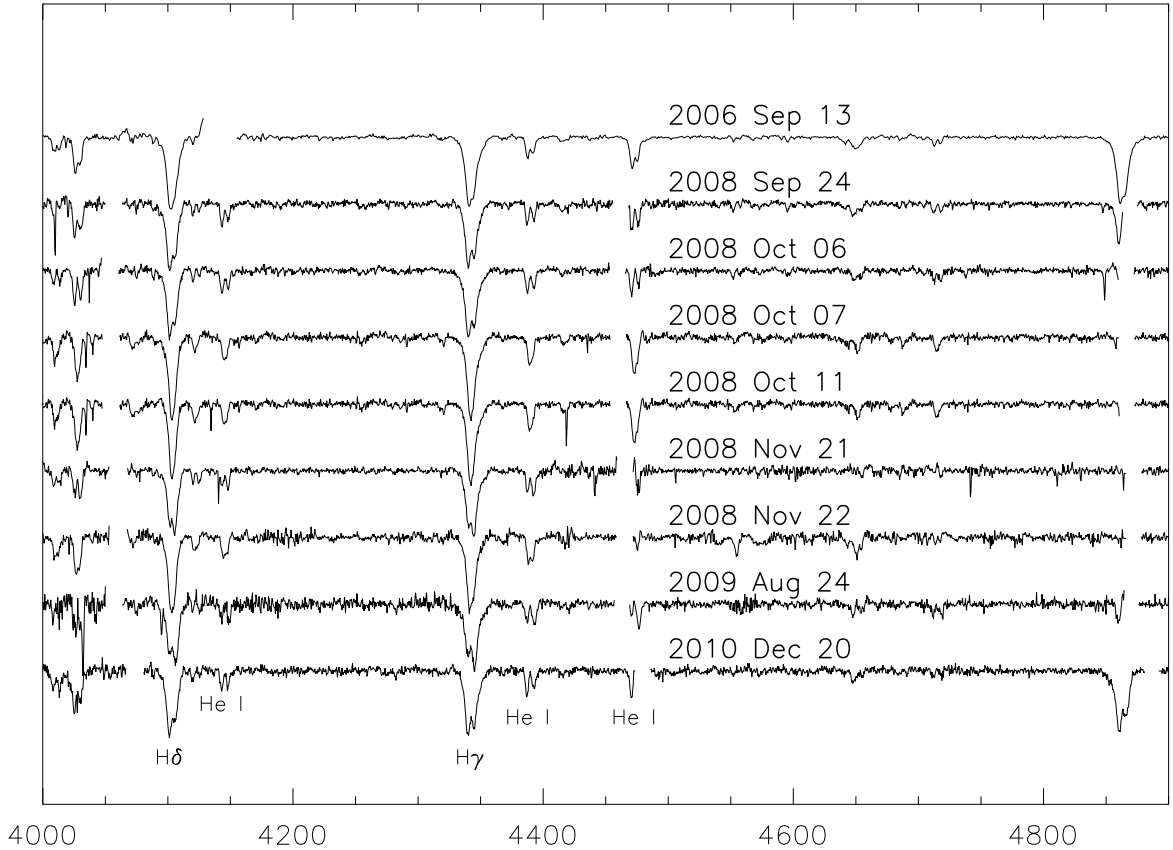


Figure 11. The multi-epoch, RIOTS4 spectra of the double-lined spectroscopic binary 27272, with observation dates shown.

of the N radial velocity measurements for each star. For three objects, more reliable values are available from fitted orbital parameters. The mean v_{sys} is 131 km s^{-1} , in good agreement with the value of 140 km s^{-1} for the Bar 1 region, where these objects are located (Figure 6).

Almost all of the stars in our monitoring sample have v_{sys} within 2σ of the mean. However, Star 5391 has $v_{\text{sys}} = 44 \text{ km s}^{-1}$, which is blueshifted by 87 km s^{-1} , more than 3σ from the mean and thus potentially a runaway star. This O8.5 III star is also identified as a binary by our three methods (Table 3).

4.7. Emission-line stars

A large fraction of our RIOTS4 stars turn out to be emission-line stars, mostly classical Oe/Be stars. We also identify four B supergiant stars that exhibit forbidden emission lines (Graus et al. 2012). One of these, star 29267 (AzV 154; Azzopardi et al. 1975) was a previously known sgB[e] star (Zickgraf et al. 1989). The other three stars are 46398, 62661, and 83480 (R15, R38, and R48, respectively; Feast et al. 1960). SgB[e] stars are normally defined as stars exhibiting forbidden emission lines along with strong IR dust excess. However, this strong dust emission is not present in the three RIOTS4 stars newly shown to be B[e] stars. In Graus et al. (2012), we discuss these objects in detail, demonstrating that they do show more modest, free-free near-IR emission. We propose

that they represent a new, transition class of dust-poor sgB[e] stars.

There are two Wolf-Rayet stars included in the RIOTS4 survey. They are stars 22409 and 30420, which are both identified as WN3 + abs stars by Massey & Duffy (2001). In our RIOTS4 spectra, we detect only H absorption lines for 22409, while 30420 also exhibits He II absorption (Figure 12). Massey & Duffy (2001) identify He II absorption in both objects and use the lack of He I to estimate that the absorption components correspond to O3-O4 stars.

The rest of the emission-line stars are classical Oe/Be stars, comprising $\sim 25\%$ of the O stars (Golden-Marx et al. 2015) and $\sim 50\%$ of the B stars in the RIOTS4 survey. These objects exhibit emission in their Balmer lines due to ‘decretion disks’ of material that are likely caused by rapid stellar rotation (e.g., Porter & Rivinius 2003). Oe/Be stars are more common at lower metallicities, with a Galactic Oe/O-star fraction of 0.03 ± 0.01 as measured from Galactic O Star Spectroscopic Survey (GOSSS; Sota et al. 2011, 2014) and a 0.24 ± 0.09 Oe/O-star fraction in SMC clusters (Martayan et al. 2010). The denominators here represent all O stars, including Oe stars. Similarly, the Be/B frequency of 30–40% in SMC clusters is about twice the Galactic frequency (Maeder et al. 1999; Wisniewski & Bjorkman 2006). This metallicity effect

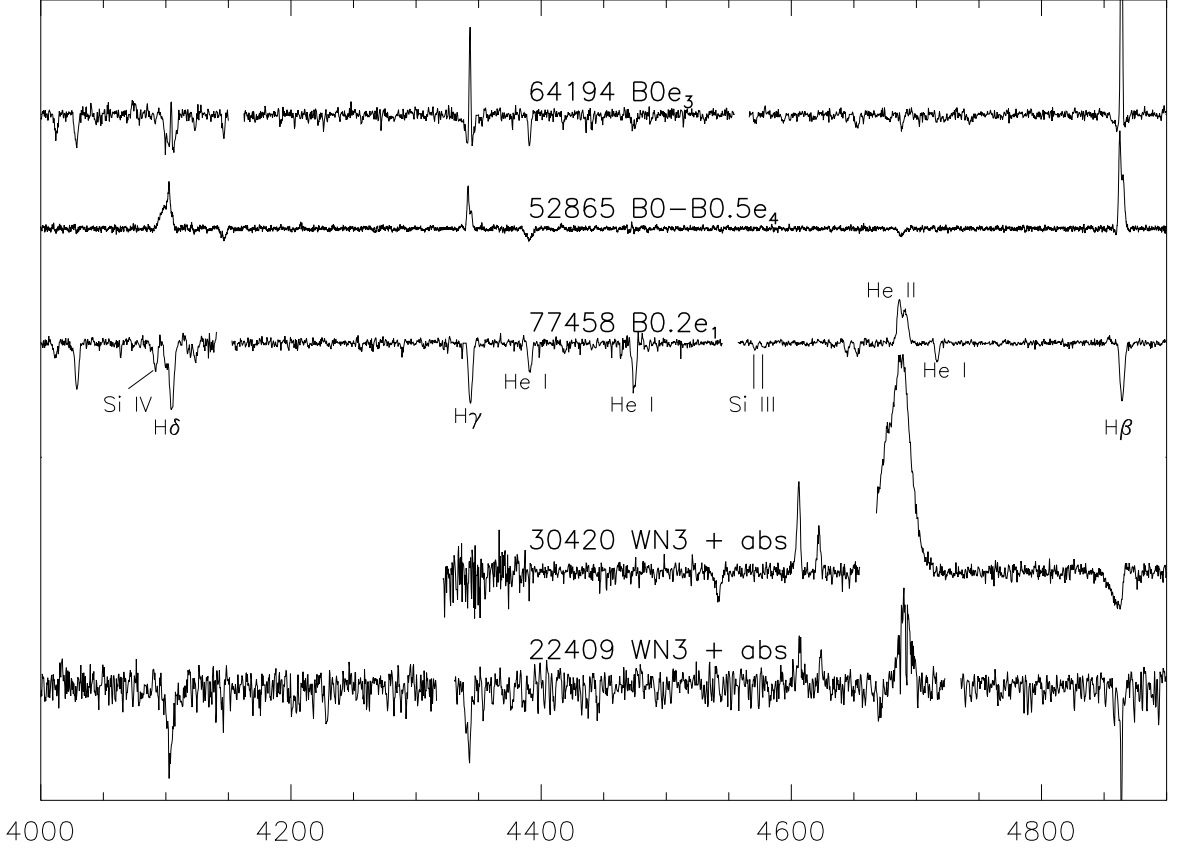


Figure 12. Spectra of the Wolf-Rayet and Be/X-ray binary stars in the RIOTS4 catalog.

is consistent with the decretion disk scenario, since the metal-poor SMC stars have weak stellar winds, thereby impeding the loss of stellar angular momentum through the winds. The high rotation rates therefore promote the formation of decretion disks, leading to the Be phenomenon.

Our RIOTS4 field Oe stars and their statistics are presented by Golden-Marx et al. (2015), yielding an Oe/O ratio of 0.27 ± 0.04 . We also find that the Oe spectral type distribution extends to earlier types than in the Galaxy, both in terms of conventional classifications and hot Oe stars whose spectral types are uncertain but are apparently of extremely early type. One extreme star, 77616, has He II in emission from the disk, showing that even the hottest O stars can present the Oe/Be phenomenon; this supports theoretical models predicting that fast rotators can reach higher effective temperatures (Brott et al. 2011). Our large sample of Oe stars in the SMC strongly supports the metallicity effects predicted by the decretion disk model and characterizes the properties of early Oe stars.

Regarding the Be stars, the RIOTS4 Be/B fraction appears to be even higher than found in previous studies. This result should be treated with caution because our sample selection criteria may be biased to favor selection of Be stars. These objects emit strongly in H α , which results in a brightening of their R magnitude, thus low-

ering Q_{UBR} . Therefore, our sample selection criterion of $Q_{UBR} \leq -0.84$ is especially useful for selecting Be stars. Given our additional limiting B magnitude criterion, it is unclear whether our completeness limit for Be stars extends to later spectral types than normal stars, or whether it provides more complete identification of B stars by including more Be stars down to the magnitude limit. A comprehensive treatment of the Be stars, including detailed investigation of the selection effects and estimates of the luminosity classes, will be presented in a future publication. For now, we include Lesh (1968) classifications (Table 1) for these stars, which are a measure of the magnitude of the Be phenomenon, and also indicate the presence of Fe II emission. In total, the Oe/Be stars account for 157 of the 374 stars (42%) in the RIOTS4 sample.

We also observed three previously known Be/X-ray binary systems within our survey, whose spectra are plotted in Figure 12. Object 52865 is reported to be a B0-0.5 III-Ve star in a binary system with a 967-s pulsar (Schurch et al. 2007; Haberl et al. 2008), and our spectral type for 52865 agrees with this spectral classification. Coe et al. (2012) report object 64194 to be a B0.5-1 Ve star in a binary system with a presumed neutron star, although no pulsar has been identified; we find a spectral type of B0e₃ for this star. Object 77458 is an eclipsing X-ray binary with a period of ~ 3.9 days (Schreier et al.

1972). Webster et al. (1972) first identified 77458 as the optical counterpart of the X-ray source, a 0.72-s pulsar (Lucke et al. 1976) with a period of 3.9 days. There is a variety of spectral classifications for 77458 in the literature, ranging from O9.5 II (Lennon 1997) to B2 I (Garmany et al. 1987), which suggest some real variation in this object’s spectrum. The most recently published spectral type is O9.7 Ia+ from Evans et al. (2004); our spectral type for this object is slightly later, B0.2e₁.

5. DISCUSSION

The RIOTS4 survey provides a first, quantitative characterization of the field massive star population based on a complete, uniformly selected sample of OB stars. It is also the first complete survey of field massive stars in an external galaxy. The resulting characterization of this population is necessarily sensitive to our definition of field stars, recalling that our criterion requires that members be at least 28 pc from other OB candidates, regardless of the presence of lower-mass stars. Thus, most of our objects can be expected to represent the “tip of the iceberg” on low-mass clusters. On the other hand, we note that our 28-pc requirement is a more stringent criterion for isolation than is often used in other studies. This clustering length is derived from the spatial distribution of the entire OB population and represents a characteristic value for the SMC as a galaxy (Oey et al. 2004). In contrast, other studies often use more arbitrary definitions, for example, “field” OB stars in the vicinity of the 30 Doradus giant star cluster (Bressert et al. 2012) correspond to a different concept of field stars.

Oey et al. (2004) showed that the clustering law for SMC OB stars follows an N_*^{-2} power law extending down to $N_* = 1$, which corresponds to our individual RIOTS4 field OB stars, where N_* is the number of OB stars per cluster. This basically confirms that most of our sample corresponds to the “tip of the iceberg” objects, as expected. However, as discussed in detail by Oey et al. (2004), the magnitude of the $N_* = 1$ bin does suggest a slight, but difficult to quantify, enhancement above a simple extrapolation of the power law distribution. Conservatively, it is < 0.3 dex, implying that any excess “deep field” population is less than 50% of the total, and perhaps much less.

Based on Monte Carlo simulations, Lamb et al. (2010) find that observations of sparse clusters and field O stars are consistent with full sampling of the IMF up to the universal stellar upper-mass limit m_{up} . This is at odds with the steep upper IMF for the field stars found in §4.2. However, these results can be reconciled by the fact that Lamb et al. (2010) also identified the existence of an effective lower limit to N_* for normal clusters, $N_* \gtrsim 40$. This value corresponds to a mean cluster mass limit of $M_{\text{cl}} \gtrsim 20 M_{\odot}$ for a Kroupa (2001) IMF. Since typically $m_{\text{up}} \gtrsim M_{\text{cl}}$ here, it is apparent that in this regime it becomes physically impossible, *on average*, to fully sample the IMF up to m_{up} . Therefore, the maximum stellar masses in the sparsest clusters must necessarily be lower, on average, than in normal clusters. *Since our RIOTS4 sample is dominated by such stars in sparse clusters, the steeper IMF is a natural consequence.* This effect also provides a natural explanation for the value of the steeper Salpeter IMF slope in clusters, compared with a simple -2 power law expected from simple Bondi-Hoyle accretion

(Oey 2011).

Our RIOTS4 field stars therefore consist of both “tip of the iceberg” stars that dominate small, but normal, clusters and “deep field” objects that are substantially more isolated. The former correspond to objects that are consistent with stochastic sampling of the IMF and clustering mass function, as described above; while the latter correspond to objects that formed in greater isolation, if any, and runaway stars.

As discussed in §4.6, Mason et al. (2009) estimate, based on somewhat uncertain statistics, that Galactic field stars have a binary frequency of about 51%, as compared with a cluster frequency of 75%. If we assume that binaries actually form with the same frequency in the field and clusters (i.e., 75%), then the lower observed field frequency can be attributed entirely to dilution by runaway stars, which increase the number of single stars. While dynamical ejection mechanisms do predict some binary runaways, these should be relatively insignificant for our purposes. These assumptions imply that runaways comprise 1/3 of all the massive field stars. If we further assume to first order that the tip-of-the-iceberg stars comprise another 50% of the field, as described above, then the remaining 1/6 of the sample corresponds to objects that formed in extreme isolation. We stress that these estimates are subject to substantial, unknown uncertainties, and they only represent a first attempt at understanding the field partition between these components. For example, if the runaway frequency is less than 33%, this implies that field stars actually form with a lower binary frequency in the field.

Thus, the possibility remains that on the order of 1/6 of the field OB stars may constitute a population that formed in extreme, or even complete, isolation. As described in §4.3, Oey et al. (2013) presented 14 candidate field stars that appear to have formed in situ, and 5 of these remain candidate members of this extremely isolated class. Lamb et al. (2010) also presented 3 such isolated candidate objects. Thus we have at least 8 candidate in-situ, deep-field OB stars, which may be around 13% of all such objects in our sample, based on the crude estimate above of their contribution to the RIOTS4 survey. As noted earlier, a number of other studies have also identified strong candidates for isolated OB star formation in the Magellanic Clouds and the Galaxy (e.g., Selier et al. 2011; Bressert et al. 2012; Oskinova et al. 2013).

In § 4.5, we found a lower limit to the runaway frequency of $\sim 11\%$, which is consistent with our estimate of $\sim 33\%$, following our analysis above. Also, the steep upper IMF (§4.2) suggests that runaway stars do not dominate the field population. Since O stars have a higher observed runaway frequency than early B stars (Gies 1987; Stone 1991), the presence of runaways counteracts the IMF steepening discussed earlier. This is also consistent with the relatively high binary frequency (0.59 ± 0.12 ; §4.6.4) in our monitoring subsample.

Thus, the picture of the field stellar population that emerges from RIOTS4 and its ancillary studies is one that is dominated by “tip of the iceberg” clusters, but with a significant fraction, on the order of one-third, of runaway stars. There is also evidence consistent with a significant contribution, perhaps $\sim 17\%$, from stars formed in extreme isolation. Work is currently in

progress to evaluate the relative contributions of these components in the RIOTS4 survey. At present, the evidence remains consistent with highly isolated OB star formation constituting a small fraction of the deep field.

6. CONCLUSIONS

The Runaways and Isolated O-Type Star Spectroscopic Survey of the SMC (RIOTS4) provides a spatially complete, spectroscopic dataset for the field massive stars in the Small Magellanic Cloud obtained from uniform criteria applied to the entire star-forming body of this galaxy. This survey sample is identified using photometric selection criteria combined with a friends-of-friends algorithm to identify the most isolated objects (Oey et al. 2004). Over the course of five years, we obtained spectra for all targets using the IMACS and MIKE spectrographs on the Magellan Telescopes. From these spectra, we derive each star’s spectral classification and radial velocity.

Using RIOTS4, we derived physical parameters such as the stellar effective temperatures and masses, allowing us to investigate the shape of the field IMF above $20M_{\odot}$ (Lamb et al. 2013). We find that the slope of the field massive star IMF is significantly steeper ($\Gamma=2.3\pm0.4$) than the traditional Salpeter slope ($\Gamma=1.35$). This result is consistent with the $\Gamma=1.8$ IMF slope found by Parker et al. (1998) and qualitatively corroborates previous observations of a steep field IMF slope of $\Gamma \sim 3 - 4$ in the Magellanic Clouds (Massey et al. 1995; Massey 2002). Complete details are given by Lamb et al. (2013).

We also use RIOTS4 data to probe limits of the most massive stars that can form in isolation or within sparsely populated clusters (Lamb et al. 2010; Oey et al. 2013). In conjunction with *HST* and ground-based imaging, we identify sparse clusters associated with target OB stars in the RIOTS4 sample. With cluster mass estimates and RIOTS4 stellar masses, we examine the relationship between the most massive star in a cluster and the mass of the parent cluster. Our results are consistent with cluster mass being independent of the most massive member star. This applies unless the total cluster masses are so small that stars near the upper-mass limit cannot form. This suppression of the most massive stars in the smallest clusters explains the steep field IMF observed above. We also identify a compelling sample of candidate field OB stars that may have formed in situ, given their apparent lack of runaway velocities and central location within dense H II regions (Oey et al. 2013).

We use the radial velocities of RIOTS4 stars to examine the large-scale velocity structure of the SMC, and for an initial look at the kinematics of the field OB population and runaway frequency. We find that the kinematics mirror those of other surveys of massive stars (Evans & Howarth 2008) and gas (Stanimirović et al. 2004). We find the systemic velocity of the SMC is $\sim 150 \text{ km s}^{-1}$, with a large velocity gradient as a function of position that roughly follows the gradient observed in H I gas (Stanimirović et al. 2004). Given this large velocity gradient, we must consider the line-of-sight SMC systemic velocity as given by the gas kinematics when identifying runaway stars within our survey. Thus, we compare the stellar radial velocity for each RIOTS4 star with the local H I gas velocity in the line of sight from Stanimirović et al. (1999). Runaway candidates are defined to be those objects with a difference $> 30 \text{ km s}^{-1}$

between stellar and H I radial velocities. We find that 11% of the sample meets this criterion, which is a lower bound due to our inability to detect transverse runaways. The identification of a binary runaway system and a candidate high-velocity (200 km s^{-1}) runaway star suggest that dynamical ejection is a significant and possibly dominant contributor to the runaway OB population.

To identify binary stars within our sample, we look for stellar radial velocity variations using 9 – 16 epochs of data for three IMACS multi-slit fields encompassing 29 stars. We use three methods to identify binary stars. First, binaries are likely to be those objects that exhibit large radial velocity variations whose amplitudes correlate with time interval. Second, we identify binary candidates using a statistical F-test, comparing the observed velocity variation with that expected from observational uncertainties (Duquennoy & Mayor 1991). Third, we identify candidates using the periodicity power spectrum and then fitting for orbital solutions. All three methods find 10 out of 17 normal OB stars ($59\% \pm 12\%$) to be strong binary candidates. This can be compared with the binary fraction found in Galactic clusters and OB associations, which is $\sim 60 - 80\%$, and that for Galactic field stars, which is $\sim 40 - 50\%$.

The RIOTS4 sample also includes a large number of emission-line stars, including two Wolf-Rayet stars and a newly identified population of dust-poor B[e] supergiant stars that may represent a transition class of objects (Graus et al. 2012). The remainder of the emission-line stars are classical Oe/Be stars, which occur at a higher frequency in the SMC than in the Galaxy. The RIOTS4 data clearly extend this finding to early Oe stars and to field Oe/Be stars. Our Oe/O-star frequency of 0.27 ± 0.04 in the SMC is significantly greater than the Milky Way value, and the SMC spectral type distribution also extends to the hottest effective temperatures, in contrast to Milky Way objects (Golden-Marx et al. 2015). These results support the decretion disk model for the Be phenomenon, since metal-poor stars rotate faster due to their inability to remove angular momentum via stellar winds. Similarly, our frequency of Be/B stars is higher than Galactic values, but this result may be biased by our photometric selection criteria. We will examine the RIOTS4 Be stars in a future work.

Work is also underway to evaluate the fraction of deep field objects relative to “tip of the iceberg” stars, which will further clarify the statistics of OB star formation in the sparsest regime. In addition, we have initiated follow-up spectroscopic monitoring to obtain binary star properties, including systemic velocities. These observations will yield reliable statistics for runaway stars, data on $v \sin i$, and Oe/Be star variability.

Many individuals helped make this publication a reality, including the referee, who provided thoughtful comments. Thanks to Nidia Morrell and Phil Massey for advice on radial velocity measurements, and to Thomas Bensby, Tom Brink, and Jess Werk for advice on the data reduction pipelines. Thanks to Mario Mateo for help with scheduling the binary monitoring runs and observing advice. We thank Fred Adams, Rupali Chandar, Xinyi Chen, Oleg Gnedin, Lee Hartmann, Wen-hsin Hsu, Anne Jaskot, Mario Mateo, Eric Pellegrini, and Jordan

Zastrow for helpful discussions. This work was supported by the National Science Foundation grants AST-0907758, AST-1514838; NASA grant NAG4-9248; and the University of Michigan, Rackham Graduate School.

REFERENCES

- Azzopardi, M., Vigneau, J., & Macquet, M. 1975, *A&AS*, 22, 285
- Battinelli, P. 1991, *A&A*, 244, 69
- Bernstein, R., Shectman, S. A., Gunnels, S. M., Mochnacki, S., & Athey, A. E. 2003, in *Society of Photo-Optical Instrumentation Engineers (SPIE) Conference Series*, Vol. 4841, *Instrument Design and Performance for Optical/Infrared Ground-based Telescopes*, ed. M. Iye & A. F. M. Moorwood, 1694–1704
- Bigelow, B. C., & Dressler, A. M. 2003, in *Society of Photo-Optical Instrumentation Engineers (SPIE) Conference Series*, Vol. 4841, *Society of Photo-Optical Instrumentation Engineers (SPIE) Conference Series*, ed. M. Iye & A. F. M. Moorwood, 1727–1738
- Blaauw, A. 1961, *Bull. Astron. Inst. Netherlands*, 15, 265
- Bonnell, I. A., Vine, S. G., & Bate, M. R. 2004, *MNRAS*, 349, 735
- Bressert, E., et al. 2012, *A&A*, 542, A49
- Brott, I., et al. 2011, *A&A*, 530, A115
- Cardelli, J. A., Clayton, G. C., & Mathis, J. S. 1989, *ApJ*, 345, 245
- Coe, M. J., et al. 2012, *MNRAS*, 424, 282
- de Wit, W. J., Testi, L., Palla, F., & Zinnecker, H. 2005, *A&A*, 437, 247
- Duquennoy, A., & Mayor, M. 1991, *A&A*, 248, 485
- Elmegreen, B. G. 2000, *ApJ*, 530, 277
- Evans, C. J., & Howarth, I. D. 2008, *MNRAS*, 386, 826
- Evans, C. J., Howarth, I. D., Irwin, M. J., Burnley, A. W., & Harries, T. J. 2004, *MNRAS*, 353, 601
- Feast, M. W., Thackeray, A. D., & Wesselink, A. J. 1960, *MNRAS*, 121, 337
- Garmany, C. D., Conti, P. S., & Massey, P. 1987, *AJ*, 93, 1070
- Gies, D. R. 1987, *ApJS*, 64, 545
- Golden-Marx, J. B., Oey, M. S., Lamb, J. B., Graus, A. S., & White, A. S. 2015, *ApJ*, submitted
- Graus, A. S., Lamb, J. B., & Oey, M. S. 2012, *ApJ*, 759, 10
- Gudehus, D. H. 2001, in *Bulletin of the American Astronomical Society*, Vol. 33, *American Astronomical Society Meeting Abstracts #198*, 850
- Gvaramadze, V. V., Gualandris, A., & Portegies Zwart, S. 2009, *MNRAS*, 396, 570
- Gvaramadze, V. V., Weidner, C., Kroupa, P., & Pflamm-Altenburg, J. 2012, *MNRAS*, 424, 3037
- Haberl, F., Eger, P., & Pietsch, W. 2008, *A&A*, 489, 327
- Harries, T. J., Hilditch, R. W., & Howarth, I. D. 2003, *MNRAS*, 339, 157
- Hoogerwerf, R., de Bruijne, J. H. J., & de Zeeuw, P. T. 2001, *A&A*, 365, 49
- Kiminki, D. C., & Kobulnicky, H. A. 2012, *ApJ*, 751, 4
- Kiminki, D. C., et al. 2012, *ApJ*, 747, 41
- Kobulnicky, H. A., et al. 2014, *ApJS*, 213, 34
- Koen, C. 2006, *MNRAS*, 365, 590
- Kratzer, K. M., Matzner, C. D., & Krumholz, M. R. 2008, *ApJ*, 681, 375
- Kratzer, K. M., Matzner, C. D., Krumholz, M. R., & Klein, R. I. 2010, *ApJ*, 708, 1585
- Kroupa, P. 2001, *MNRAS*, 322, 231
- Krumholz, M. R., Klein, R. I., McKee, C. F., Offner, S. S. R., & Cunningham, A. J. 2009, *Science*, 323, 754
- Lada, C. J., & Lada, E. A. 2003, *ARA&A*, 41, 57
- Lamb, J. B., Oey, M. S., Graus, A. S., Adams, F. C., & Segura-Cox, D. M. 2013, *ApJ*, 763, 101
- Lamb, J. B., Oey, M. S., Werk, J. K., & Ingleby, L. D. 2010, *ApJ*, 725, 1886
- Lennon, D. J. 1997, *A&A*, 317, 871
- Leonard, P. J. T., & Duncan, M. J. 1990, *AJ*, 99, 608
- Lesh, J. R. 1968, *ApJS*, 17, 371
- Lucke, R., Yentis, D., Friedman, H., Fritz, G., & Shulman, S. 1976, *ApJ*, 206, L25
- Maeder, A., Grebel, E. K., & Mermilliod, J.-C. 1999, *A&A*, 346, 459
- Maíz-Apellániz, J., Walborn, N. R., Galué, H. Á., & Wei, L. H. 2004, *ApJS*, 151, 103
- Martayan, C., Baade, D., & Fabregat, J. 2010, *A&A*, 509, A11
- Mason, B. D., Gies, D. R., Hartkopf, W. I., Bagnuolo, Jr., W. G., ten Brummelaar, T., & McAlister, H. A. 1998, *AJ*, 115, 821
- Mason, B. D., Hartkopf, W. I., Gies, D. R., Henry, T. J., & Helsel, J. W. 2009, *AJ*, 137, 3358
- Massey, P. 2002, *ApJS*, 141, 81
- Massey, P. 2011, in *Astronomical Society of the Pacific Conference Series*, Vol. 440, *UP2010: Have Observations Revealed a Variable Upper End of the Initial Mass Function?*, ed. M. Treyer, T. Wyder, J. Neill, M. Seibert, & J. Lee, 29
- Massey, P., & Duffy, A. S. 2001, *ApJ*, 550, 713
- Massey, P., Lang, C. C., Degioia-Eastwood, K., & Garmany, C. D. 1995, *ApJ*, 438, 188
- McSwain, M. V., Ransom, S. M., Boyajian, T. S., Grundstrom, E. D., & Roberts, M. S. E. 2007, *ApJ*, 660, 740
- Negueruela, I., Steele, I. A., & Bernabeu, G. 2004, *Astronomische Nachrichten*, 325, 749
- Oey, M. S. 2011, *ApJ*, 739, L46
- Oey, M. S., King, N. L., & Parker, J. W. 2004, *AJ*, 127, 1632
- Oey, M. S., Lamb, J. B., Kushner, C. T., Pellegrini, E. W., & Graus, A. S. 2013, *ApJ*, 768, 66
- Oskinova, L. M., Steinke, M., Hamann, W.-R., Sander, A., Todt, H., & Liermann, A. 2013, *MNRAS*, 436, 3357
- Parker, J. W., et al. 1998, *AJ*, 116, 180
- Parker, J. W., Zaritsky, D., Stecher, T. P., Harris, J., & Massey, P. 2001, *AJ*, 121, 891
- Portegies Zwart, S. F. 2000, *ApJ*, 544, 437
- Porter, J. M., & Rivinius, T. 2003, *PASP*, 115, 1153
- Poveda, A., Ruiz, J., & Allen, C. 1967, *Boletín de los Observatorios Tonantzintla y Tacubaya*, 4, 86
- Roberts, D. H., Lehar, J., & Dreher, J. W. 1987, *AJ*, 93, 968
- Sahade, J. 1959, *PASP*, 71, 151
- Sana, H., Gosset, E., & Evans, C. J. 2009, *MNRAS*, 400, 1479
- Sana, H., Gosset, E., Nazé, Y., Rauw, G., & Linder, N. 2008, *MNRAS*, 386, 447
- Sana, H., James, G., & Gosset, E. 2011, *MNRAS*, 416, 817
- Schmidt-Kaler, T. 1982, *Bulletin d'Information du Centre de Données Stellaires*, 23, 2
- Schreier, E., Giacconi, R., Gursky, H., Kellogg, E., & Tananbaum, H. 1972, *ApJ*, 178, L71
- Schurch, M. P. E., et al. 2007, *MNRAS*, 381, 1561
- Selzer, R., Heydari-Malayeri, M., & Gouliermis, D. A. 2011, *A&A*, 529, A40
- Selman, F. J., Espinoza, P., & Melnick, J. 2011, in *Astronomical Society of the Pacific Conference Series*, Vol. 440, *UP2010: Have Observations Revealed a Variable Upper End of the Initial Mass Function?*, ed. M. Treyer, T. Wyder, J. Neill, M. Seibert, & J. Lee, 39
- Shu, F. H., Adams, F. C., & Lizano, S. 1987, *ARA&A*, 25, 23
- Sota, A., Maíz Apellániz, J., Morrell, N. I., Barbá, R. H., Walborn, N. R., Gamen, R. C., Arias, J. I., & Alfaro, E. J. 2014, *ApJS*, 211, 10
- Sota, A., Maíz Apellániz, J., Walborn, N. R., Alfaro, E. J., Barbá, R. H., Morrell, N. I., Gamen, R. C., & Arias, J. I. 2011, *ApJS*, 193, 24
- Stanimirović, S., Staveley-Smith, L., Dickey, J. M., Sault, R. J., & Snowden, S. L. 1999, *MNRAS*, 302, 417
- Stanimirović, S., Staveley-Smith, L., & Jones, P. A. 2004, *ApJ*, 604, 176
- Stone, R. C. 1981, *AJ*, 86, 544
- . 1991, *AJ*, 102, 333
- Struve, O. 1937, *ApJ*, 85, 41
- Testi, L., Palla, F., & Natta, A. 1998, *A&AS*, 133, 81
- Testi, L., Palla, F., Prusti, T., Natta, A., & Maltagliati, S. 1997, *A&A*, 320, 159
- Udalski, A., Szymanski, M., Kubiak, M., Pietrzynski, G., Wozniak, P., & Zebrun, K. 1998, *Acta Astron.*, 48, 147
- van den Bergh, S. 2004, *AJ*, 128, 1880
- Walborn, N. R., & Fitzpatrick, E. L. 1990, *PASP*, 102, 379
- Walborn, N. R., Lennon, D. J., Haser, S. M., Kudritzki, R.-P., & Voels, S. A. 1995, *PASP*, 107, 104
- Walborn, N. R., Lennon, D. J., Heap, S. R., Lindler, D. J., Smith, L. J., Evans, C. J., & Parker, J. W. 2000, *PASP*, 112, 1243
- Walborn, N. R., Nichols, J. S., & Waldron, W. L. 2009, *ApJ*, 703, 633

- Webster, B. L., Martin, W. L., Feast, M. W., & Andrews, P. J. 1972, *Nature Physical Science*, 240, 183
- Weidner, C., & Kroupa, P. 2006, *MNRAS*, 365, 1333
- Wisniewski, J. P., & Bjorkman, K. S. 2006, *ApJ*, 652, 458
- Zaritsky, D., Harris, J., Thompson, I. B., Grebel, E. K., & Massey, P. 2002, *AJ*, 123, 855
- Zickgraf, F.-J., Wolf, B., Stahl, O., & Humphreys, R. M. 1989, *A&A*, 220, 206
- Zinnecker, H. 1982, *Annals of the New York Academy of Sciences*, 395, 226

Table 1. RIOTS4 Catalog^a

ID ^b	B^b	V^b	Q_{UBR}	A_V^c	Sp Type	RV_{star} (km s ⁻¹)	RV_{HI}^d (km s ⁻¹)	Instrument	Observation Date (YYMMDD)
107	14.96	15.00	-0.95	0.82	Be ₃	–	–	MIKE	111024
298	15.18	15.12	-0.91	1.03	B1e ₃₊	–	–	IMACS f/4	070920
1037	15.15	15.28	-0.85	0.44	B0.5 V	110	110	IMACS f/4	070920
1600	14.42	14.60	-0.87	0.32	O8.5 V	93	103	IMACS f/4	070920
1631	15.19	15.15	-0.99	1.11	B1e ₂	120	120	IMACS f/4	070920
1830	13.84	13.94	-0.85	0.49	B0.5 III	–	–	IMACS f/4	070920
1952	14.98	14.93	-0.91	1.09	B1e ₂	80	97	IMACS f/4	070920
2034	14.51	14.57	-1.01	0.78	B	–	–	MIKE	111024
2093	15.12	15.19	-0.95	0.68	B1e ₃₊	–	–	IMACS f/4	070920
2666	15.15	15.18	-0.88	0.70	B1.5e ₃₊	117	117	IMACS f/4	081007
3173	14.66	14.37	-1.73	0.99	O3-4 + neb	111	111	IMACS f/4	081011
3224	14.86	14.70	-0.92	1.39	B1e ₂₊	102	102	IMACS f/4	070920
3459	13.32	13.46	-0.93	0.48	O9.5 I	201	169	IMACS f/4	081011
3722	15.20	14.83	-1.08	0.46	B	–	–	IMACS f/4	081007
3815	14.97	14.92	-1.02	1.13	Be ₂	–	–	IMACS f/4	081007
4294	14.96	15.00	-0.93	0.78	Be ₂	–	–	MIKE	111024
4424	14.70	14.82	-0.90	0.49	B0 III	–	–	IMACS f/4	081011
4919	13.66	13.85	-0.95	0.33	B0 III	118	118	MIKE	111024
5041	15.09	15.09	-0.96	0.96	B0 V	130	130	MIKE	111024
5063	14.66	14.60	-0.87	1.02	B1e ₃	116	116	IMACS f/4	081007
5313	14.89	15.11	-0.87	0.23	O8.5 V	135	135	IMACS f/4	081007
5905	14.87	14.90	-0.91	0.75	B0e ₂	–	–	IMACS f/4	081007
6908	14.77	14.53	-1.02	1.71	O9.5-B0 III	128	128	IMACS f/4	081006 ^e
6940	14.25	14.33	-0.96	0.68	B1e ₃₊	131	131	IMACS f/4	081011
7254	14.75	14.74	-0.86	0.86	O9.5 IIIe ₂	126	126	IMACS f/4	081006 ^e
7329	14.32	14.45	-0.94	0.49	Be ₂	–	–	MIKE	111024
7437	12.93	13.12	-0.94	0.33	O6.5 I(f)	151	151	IMACS f/4	081006 ^e
7782	14.30	14.46	-0.91	0.40	O8 V	127	127	IMACS f/4	081006 ^e
8098	14.13	14.17	-1.00	0.85	B1e ₃	165	165	MIKE	111024
8609	13.98	14.11	-0.87	0.48	B0 III	128	128	IMACS f/4	081006 ^e
9732	14.63	14.81	-0.88	0.31	O7 Vz	136	136	IMACS f/4	081011
10026	14.64	14.68	-1.02	0.87	Be ₃₊	–	–	IMACS f/4	081011
10421	14.81	14.99	-0.87	0.28	B1 V	152	161	IMACS f/4	070919
10556	14.60	14.63	-0.89	0.74	B0.2 V	100	120	IMACS f/4	090825
10671	14.88	14.89	-0.84	0.85	B0.5 V	122	122	IMACS f/4	081006 ^e
11045	14.80	15.01	-0.87	0.21	O8.5 V	182	169	IMACS f/4	070919
11087	14.67	14.71	-0.93	0.80	B1e ₁	–	–	IMACS f/4	090825

Table 1—Continued

ID ^b	B^b	V^b	Q_{UBR}	A_V^c	Sp Type	RV _{star} (km s ⁻¹)	RV _{HI} ^d (km s ⁻¹)	Instrument	Observation Date (YYMMDD)
11213	14.88	14.77	-0.97	1.29	Be ₃ +	–	–	IMACS f/4	090824
11238	14.41	14.30	-0.96	1.21	O + B	–	–	MIKE	111024
11280	14.15	14.16	-0.94	0.90	B1e ₃	125	138	IMACS f/4	070919
11623	14.12	14.13	-0.86	0.83	O9 III:	170	170	IMACS f/4	060912
11677	14.47	14.46	-1.01	1.04	O9 III:e ₃ +	–	–	IMACS f/4	081011
11777	13.76	13.88	-0.92	0.53	B0.2 V	168	168	IMACS f/4	060912
11802	14.62	14.59	-0.86	0.96	B0.2 IV	155	155	IMACS f/4	090824
12102	14.64	14.69	-0.98	0.84	O9 IIIe ₂	–	–	IMACS f/4	081011
13075	12.93	13.05	-0.89	0.52	O9.5 I	131	131	IMACS f/4	060912
13314	14.76	14.77	-0.87	0.84	B1 III	168	215	IMACS f/4	070919
13682	14.94	14.92	-0.96	1.03	Be ₃	–	–	IMACS f/4	090825
13774	15.07	15.07	-0.84	0.85	–	–	–	IMACS f/4	060913
13831	13.91	14.06	-0.87	0.39	B0.5 V	172	172	IMACS f/4	060912
13896	13.56	13.76	-0.98	0.30	O8 III((f))	159	163	IMACS f/4	081011
14324	14.17	14.11	-0.97	1.12	O6 V((f))e ₂	152	152	IMACS f/4	090824
14878	14.11	14.25	-0.89	0.46	O9 III	147	147	IMACS f/4	090825
15060	14.11	14.29	-0.88	0.30	B0.2 III-IV	155	155	IMACS f/4	060912
15102	15.17	15.01	-0.89	1.40	B1.5 V	103	123	IMACS f/4	081011
15256	15.09	15.00	-0.90	1.14	B1 V	157	157	IMACS f/4	060912
15263	15.05	15.22	-0.87	0.28	B0.2 V	109	156	IMACS f/4	070919
15271	13.36	13.54	-0.94	0.39	O6 III((f))e ₁	143	153	IMACS f/4	070919
15618	14.84	14.95	-0.92	0.53	B	128	128	IMACS f/4	090825
15742	13.51	13.64	-0.92	0.53	O9 III	168	168	IMACS f/4	090825
15854	15.21	14.51	-1.17	0.68	B1e ₃	107	117	IMACS f/4	090824
16039	14.53	14.54	-1.03	0.99	B1e ₄ +	–	–	IMACS f/4	090825
16147	14.03	14.15	-0.91	0.53	B0 V	147	147	IMACS f/4	060912
16230	13.01	13.20	-0.90	0.29	O9 III:	71	136	IMACS f/4	060912
16481	14.16	14.26	-0.94	0.62	O9.5 V	160	160	IMACS f/4	070919
16518	13.77	13.90	-0.96	0.53	B0 V	176	171	IMACS f/4	070919
16587	13.99	13.91	-1.00	1.24	B0 V	–	–	IMACS f/4	070920
16616	14.18	14.29	-0.86	0.50	–	–	–	IMACS f/4	060913
17240	14.37	14.47	-0.85	0.55	O7.5 V	105	108	IMACS f/4	060912
17813	14.83	14.84	-0.86	0.86	B0 V	192	184	IMACS f/4	070920
18187	14.95	15.00	-0.95	0.79	Be ₂ +	–	–	IMACS f/4	070919
18301	14.40	14.58	-0.86	0.31	B0.2 V	155	155	IMACS f/4	070919
18329	14.64	14.65	-0.98	0.91	O9.5 IIIe ₄ + pec	119	123	IMACS f/4	070920
18373	13.48	13.41	-1.05	1.26	Be ₃	160	160	MIKE	111025

Table 1—Continued

ID ^b	B^b	V^b	Q_{UBR}	A_V^c	Sp Type	RV_{star} (km s ⁻¹)	RV_{HI}^d (km s ⁻¹)	Instrument	Observation Date (YYMMDD)
19382	14.27	14.31	-0.96	0.81	B0 V	153	153	IMACS f/4	070920
19728	12.49	12.59	-0.89	0.59	B1 I	166	174	IMACS f/4	070919
20939	14.14	14.18	-0.86	0.73	B1 II	155	155	IMACS f/4	060912
21844	14.09	14.18	-0.86	0.57	O8 III((f))	151	151	IMACS f/4	080920 ^e
21877	14.96	15.10	-0.95	0.46	O7 V	91	113	IMACS f/4	060912
21933	15.08	14.83	-0.92	1.69	Be ₃	130	130	IMACS f/4	081006 ^e
21983	15.18	15.18	-0.98	0.96	O9.5 V	174	174	IMACS f/4	070920
22178	13.34	13.49	-0.91	0.43	O + B	176	171	MIKE	111025
22321	13.70	13.69	-0.98	1.00	O9.5 IIIpe ₄₊	167	167	IMACS f/4	080920 ^e
22409	15.14	14.97	-1.01	1.52	WN3 + abs ^f	98	118	IMACS f/4	060912
22451	13.98	14.14	-0.93	0.41	O9 III	–	–	IMACS f/4	070920
22623	15.19	15.21	-0.86	0.84	B0e ₃	–	–	IMACS f/4	070920
23710	14.85	14.74	-0.97	1.31	O9-B0 pe ₃₊	168	168	IMACS f/4	080920 ^e
23859	14.75	14.82	-0.93	0.72	B1e ₃	–	–	IMACS f/4	060912
23954	14.59	14.58	-0.85	0.86	B1.5e ₃₊	130	130	IMACS f/4	080920 ^e
24056	13.61	13.64	-0.85	0.76	B1.5 III	199	186	IMACS f/4	070920
24096	14.56	14.53	-1.05	1.07	B0 V	138	135	IMACS f/4	060912
24119	14.78	14.80	-1.01	0.88	B0-0.2 V	–	–	IMACS f/4	070920
24213	14.17	14.34	-0.88	0.31	B0 III	126	126	IMACS f/4	080920 ^e
24229	14.79	14.80	-0.86	0.82	B1e ₂	155	155	IMACS f/4	080920 ^e
24895	14.23	14.20	-0.88	0.99	Be ₃	–	–	MIKE	111024
24914	14.19	14.19	-1.00	0.95	O9 III-Vpe ₁	81	105	IMACS f/4	081121 ^e
25282	14.73	14.74	-0.90	0.90	B0e ₁	130	130	IMACS f/4	080920 ^e
25337	15.12	15.03	-0.89	1.12	Be ₃	124	124	IMACS f/4	080920 ^e
25639	14.85	14.69	-0.96	1.42	B0.5e ₃₊	–	–	IMACS f/4	060912
25974	15.08	15.08	-0.85	0.75	B1.5 V	116	123	IMACS f/4	060912
27135	15.20	15.32	-0.93	0.56	B1e ₂	113	117	IMACS f/4	080920 ^e
27496	14.60	14.77	-0.84	0.27	B0.5 V	137	137	IMACS f/4	060912
27600	13.79	13.90	-0.89	0.53	B0.5 III	177	177	IMACS f/4	080920 ^e
27712	14.96	15.09	-0.85	0.44	B1.5 V	127	127	IMACS f/4	080920 ^e
27736	14.54	14.54	-0.99	0.95	B0e ₂	153	153	IMACS f/4	080920 ^e
27884	14.35	14.35	-1.06	1.05	O7-8.5 Vpe ₄₊	156	156	IMACS f/4	080920 ^e
28496	15.01	15.07	-0.87	0.73	B0 V	154	154	MIKE	111024
28841	14.24	14.27	-0.89	0.78	B1 III	141	141	IMACS f/4	080920 ^e
29267	13.48	13.20	-1.01	1.78	B[e]	–	–	MIKE	111024
29312	15.01	15.29	-0.87	0.00	B0.7 III	162	162	IMACS f/4	060912
30018	14.83	14.95	-0.93	0.48	B0.2 III	160	160	MIKE	111024

Table 1—Continued

ID ^b	B^b	V^b	Q_{UBR}	A_V^c	Sp Type	RV_{star} (km s ⁻¹)	RV_{HI}^d (km s ⁻¹)	Instrument	Observation Date (YYMMDD)
30420	15.12	15.24	-0.97	0.56	WN3 + abs ^f	–	–	IMACS f/4	060912
30472	14.55	14.67	-0.87	0.48	B1e ₁	–	–	IMACS f/4	060912
30492	14.45	14.51	-0.92	0.72	B0.5	179	179	MIKE	111024
30744	14.24	14.30	-0.88	0.66	B1 III + O9.5 Ve ₂	–	–	IMACS f/4	060912
31574	15.17	15.10	-0.90	1.05	B1 V	149	145	IMACS f/4	060912
31699	14.73	14.78	-0.90	0.73	B1e ₁	–	–	IMACS f/4	060912
32449	14.19	14.29	-0.86	0.51	B1.5 III	121	121	IMACS f/4	060912
32552	14.85	14.87	-0.96	0.88	B0e ₃	–	–	IMACS f/4	090825
32752	14.63	14.57	-0.90	1.04	Be ₃₊	270	186	MIKE	111025
33135	15.20	15.26	-0.95	0.77	B0e ₃₊	–	–	IMACS f/4	090825
33245	15.10	15.23	-0.91	0.47	Be ₁	–	–	IMACS f/4	060912
33823	14.45	14.62	-0.89	0.35	O9.5 III	170	170	MIKE	111025
34005	14.80	15.01	-1.02	0.29	O9.5 V	166	166	IMACS f/4	090825
34315	13.68	13.78	-0.88	0.54	B1 II	138	138	IMACS f/4	060912
34457	13.74	13.93	-0.91	0.30	B0 III	168	168	MIKE	111025
34651	15.01	14.99	-0.87	0.92	Be ₁	–	–	MIKE	111025
34988	14.84	14.85	-0.95	0.89	Be ₂	226	183	MIKE	111025
35474	14.56	14.45	-0.93	1.53	B1 III	224	184	MIKE	111025
35491	14.66	14.71	-0.90	0.77	O8 V	126	126	IMACS f/4	060911
35598	14.88	15.15	-0.94	0.05	O8 V	162	162	IMACS f/4	060911
36175	12.64	12.68	-0.85	0.73	B1 II	191	191	MIKE	111024
36213	13.21	13.38	-0.90	0.38	O9.5 III + B	120	120	MIKE	111025
36294	14.51	14.55	-0.95	0.80	B0.5e ₁	130	130	IMACS f/4	060911
36325	15.02	14.88	-0.88	1.33	O9.5 V	146	146	IMACS f/4	060912
36514	15.01	15.15	-0.87	0.47	O9 V	141	141	IMACS f/4	060911
36815	14.93	14.98	-0.96	0.78	Be ₂	155	155	MIKE	111025
36975	15.04	15.04	-0.89	0.87	Be ₄₊	164	164	MIKE	111026
37419	15.12	14.95	-0.98	1.54	Be ₄₊	127	127	IMACS f/4	060911
37502	14.65	14.62	-1.03	1.10	O9.5-B0: pe ₃₊	–	–	IMACS f/4	060911
38024	14.32	14.53	-0.94	0.27	O4 V((f))	103	151	IMACS f/4	090825
38036	14.28	14.33	-0.98	0.82	O6.5-7: Vpe ₃	152	152	IMACS f/4	060911
38445	14.67	14.68	-1.09	1.02	Be ₄₊	–	–	IMACS f/4	090825
38508	15.14	14.95	-0.96	1.52	B0.7	179	179	IMACS f/4	090825
38893	14.74	14.89	-0.90	0.41	B0e ₁	179	179	IMACS f/4	060911
38921	14.07	14.12	-0.96	0.80	B0 III	154	154	IMACS f/4	060911
39211	14.73	14.94	-0.86	0.18	O9.5 III	156	156	IMACS f/4	090825
39904	15.13	15.17	-0.98	0.81	B0e ₂	–	–	IMACS f/4	090825

Table 1—Continued

ID ^b	B^b	V^b	Q_{UBR}	A_V^c	Sp Type	RV _{star} (km s ⁻¹)	RV _{HI} ^d (km s ⁻¹)	Instrument	Observation Date (YYMMDD)
40380	14.22	14.33	-0.92	0.58	O7 V	181	178	IMACS f/4	090825
40504	13.98	14.15	-0.87	0.30	B1.5 III	95	150	IMACS f/4	090825
41183	14.78	14.84	-0.95	0.77	Be ₁	–	–	IMACS f/4	101222
41345	14.87	15.04	-0.89	0.34	B1 III	–	–	IMACS f/4	060911
41648	13.86	13.95	-0.90	0.61	B0.5 III	106	118	IMACS f/4	060911
42260	14.43	14.54	-0.85	0.50	O9.5 III	140	140	IMACS f/4	060911
42654	14.84	14.78	-0.99	1.17	Be ₃₊	–	–	IMACS f/4	090825
42959	14.59	14.72	-0.91	0.48	B	–	–	–	–
43411	14.90	14.97	-0.98	0.72	O9 V	132	150	IMACS f/4	081006
43589	14.93	15.04	-0.89	0.56	B0e ₃	–	–	IMACS f/4	060911
43724	14.05	14.25	-0.96	0.32	O7 III((f))	100	148	IMACS f/4	101222
44316	15.04	15.15	-0.93	0.58	Be ₃	192	169	MIKE	111026
44336	14.78	14.72	-1.01	1.20	B1.5e	–	–	IMACS f/4	090825
44965	14.65	14.69	-1.06	0.90	B0e ₂	–	–	IMACS f/4	070920
45640	13.95	14.01	-0.97	0.74	B1e ₂	142	150	IMACS f/4	081006
46022	14.74	14.85	-0.84	0.52	O9.5 V	148	153	IMACS f/4	101221
46035	14.05	14.24	-0.95	0.34	O7 V	–	–	IMACS f/4	101221
46090	14.58	14.66	-0.88	0.64	B0e ₂	–	–	IMACS f/4	070920
46241	15.17	15.11	-0.86	1.00	B1 V	117	117	IMACS f/4	060912
46317	14.53	14.76	-0.90	0.17	O8.5 V	174	174	IMACS f/4	070920
46392	14.39	14.56	-0.93	0.35	B0.7 IV	138	156	IMACS f/4	101222
46398	12.67	12.64	-0.94	1.00	B[e]	–	–	MIKE	111024
46831	15.05	15.15	-0.87	0.54	O7.5-9 V	145	148	IMACS f/4	081006
47029	15.08	15.18	-0.84	0.53	B0.2 V	188	188	IMACS f/4	101221
47459	15.10	15.17	-0.85	0.55	B0 V + B	155	155	IMACS f/4	060912
47478	14.74	14.96	-0.98	0.28	O7 V	143	154	IMACS f/4	101222
47668	15.04	15.16	-0.97	0.56	Be	–	–	–	–
47908	14.64	14.19	-1.10	0.52	Be	–	–	IMACS f/4	090824
48037	14.56	14.54	-1.00	1.03	B0e ₃	–	–	IMACS f/4	090824
48057	14.91	14.93	-0.97	0.87	B0.2e ₃₊	–	–	IMACS f/4	090824
48170	14.16	14.29	-0.96	0.53	O9.5 V	145	145	IMACS f/4	081011
48266	15.19	15.17	-1.08	1.06	B0e ₃₊	–	–	IMACS f/4	081006
48432	14.94	15.07	-0.90	0.37	B0III + B	201	186	MIKE	111025
48601	13.58	13.71	-0.92	0.49	B0 III	133	133	IMACS f/4	060912
48882	15.19	15.16	-0.99	1.04	B1e ₃₊	148	158	IMACS f/4	090824
49014	14.53	14.60	-0.95	0.69	B0e ₃₊	133	133	IMACS f/4	090824
49450	14.07	14.22	-0.86	0.37	O9.5 V	150	156	IMACS f/4	101222

Table 1—Continued

ID ^b	B^b	V^b	Q_{UBR}	A_V^c	Sp Type	RV _{star} (km s ⁻¹)	RV _{HI} ^d (km s ⁻¹)	Instrument	Observation Date (YYMMDD)
49517	15.02	14.97	-0.96	1.11	B1.5 V	138	138	IMACS f/4	060912
49580	14.22	14.38	-0.88	0.39	O9.5 IV	124	124	IMACS f/4	090824
49825	14.75	14.94	-0.88	0.29	B0.2 III	140	156	IMACS f/4	101222
49937	15.14	15.19	-0.90	0.74	B0V	395	192	MIKE	111025
50095	14.48	14.51	-0.94	0.87	O9 Ve ₄₊	–	–	IMACS f/4	060912
50153	14.64	14.46	-1.47	1.92	H II region	–	–	MIKE	111025
50331	12.83	12.99	-0.92	0.41	–	–	–	IMACS f/4	060912
50396	15.17	15.16	-1.00	1.00	Be ₂	–	–	IMACS f/4	090824
50609	12.43	12.55	-0.90	0.53	B1 I	149	141	IMACS f/4	090824
50791	15.04	15.19	-0.93	0.47	O8 V	190	183	IMACS f/4	081007
50825	14.58	14.84	-0.92	0.08	O8 V	230	186	IMACS f/4	101222
51036	15.10	15.16	-0.87	0.71	Be ₁	–	–	IMACS f/4	101222
51214	14.72	14.76	-1.03	0.87	Be ₃	–	–	IMACS f/4	081006
51234	13.58	13.66	-0.86	0.58	B1.5 III	187	187	IMACS f/4	070920
51236	14.93	14.92	-0.89	0.89	Be ₄₊	–	–	IMACS f/4	090824
51373	13.72	13.79	-1.08	0.84	O8 IIIze ₃	–	–	IMACS f/4	090824
51384	13.26	13.42	-0.92	0.44	O9.5 Ia	82	123	IMACS f/4	070920
51419	15.15	15.29	-0.90	0.45	O9 III	–	–	IMACS f/4	060912
51424	14.99	15.02	-0.94	0.82	B1e ₃₊	151	153	IMACS f/4	081007
51435	14.92	15.12	-0.89	0.29	O9 III-V	195	189	IMACS f/4	090824
51500	14.72	14.97	-0.93	0.15	O6 V	171	171	IMACS f/4	101221
52257	14.57	14.61	-0.87	0.77	B0e ₃	–	–	IMACS f/4	090824
52363	14.80	14.98	-0.97	0.38	O7 III((f))e ₁	170	170	IMACS f/4	101222
52410	13.69	13.75	-1.07	0.85	O8 III: ze ₃ pec	–	–	IMACS f/4	090824
52865	14.48	14.56	-1.12	0.85	B0-B0.5e ₄	192	181	MIKE	111025
52959	15.03	15.25	-0.87	0.14	B0 V	–	–	MIKE	111026
53042	14.67	14.85	-0.86	0.28	O9.5 V	154	163	IMACS f/4	090824
53319	14.66	14.90	-0.87	0.15	B0 V	173	173	IMACS f/4	081007
53360	15.04	15.09	-0.95	0.77	O7-9p:e ₂	–	–	IMACS f/4	101222
53480	13.99	14.24	-1.15	0.03	–	–	–	–	–
54456	13.35	13.55	-0.88	0.25	B0 III	138	161	IMACS f/4	101222
54721	12.69	12.88	-0.95	0.35	O9 III	118	151	IMACS f/4	081007
55417	14.58	14.62	-0.99	0.83	B1e ₄₊	–	–	IMACS f/4	070920
55952	14.43	14.64	-0.89	0.21	B0.2 V	251	196	IMACS f/4	081007
56503	14.87	14.95	-0.92	0.68	O9 Ve ₂	–	–	IMACS f/4	070920
56587	14.68	14.75	-0.97	0.73	B0 V	–	–	IMACS f/2	110721
56662	14.87	11.85	-1.30	0.54	B	182	182	MIKE	111026

Table 1—Continued

ID ^b	B^b	V^b	Q_{UBR}	A_V^c	Sp Type	RV_{star} (km s ⁻¹)	RV_{HI}^d (km s ⁻¹)	Instrument	Observation Date (YYMMDD)
57397	14.66	14.69	-0.96	0.82	B1e ₃₊	158	163	IMACS f/4	070920
58168	14.94	14.87	-0.89	1.10	–	–	–	–	–
58756	14.79	14.74	-0.94	1.08	Be ₃₊	–	–	IMACS f/4	081011
58864	15.14	15.14	-0.91	0.90	B0e ₃	–	–	IMACS f/4	070920
58947	13.63	13.63	-0.85	0.74	B1 III	156	164	IMACS f/4	081011
59319	14.23	14.32	-0.99	0.68	early Ope ₃	–	–	IMACS f/4	081007
59421	13.64	13.78	-0.86	0.42	B1 III	155	146	IMACS f/4	081011
59867	14.83	14.76	-1.06	1.25	B0e ₃₊	–	–	IMACS f/4	070920
59897	15.19	15.28	-0.93	0.66	B0e ₃	154	148	MIKE	111026
59977	14.81	14.81	-0.98	0.94	B0e ₁	–	–	IMACS f/2	110721
60439	13.73	13.94	-0.90	0.22	O + B	–	–	MIKE	111026
60460	14.74	14.98	-0.88	0.09	O8.5 V	173	173	IMACS f/4	081011
61039	14.87	15.11	-0.85	0.09	O9.5 V	184	184	IMACS f/4	081007
61543	15.11	15.19	-0.85	0.61	B	–	–	MIKE	111025
61842	13.38	13.47	-0.87	0.59	B1 III	–	–	IMACS f/2	110719
62416	14.59	14.68	-0.92	0.61	O9 V	135	135	IMACS f/4	070920
62638	14.57	14.67	-0.98	0.65	O9.5 III-Ve ₂	–	–	IMACS f/4	081007
62661	13.01	12.98	-0.85	0.91	B[e]	89	159	MIKE	111026
62981	14.66	14.86	-0.87	0.24	B0.2 V	160	166	IMACS f/4	070920
63112	14.97	14.99	-0.90	0.82	B0.5e ₃₊	113	159	IMACS f/4	081007
63284	13.38	13.49	-0.85	0.50	B1e ₃₊	124	161	IMACS f/4	070920
63413	13.97	13.90	-0.89	1.10	O9.5 Ia	144	163	IMACS f/4	081007
63842	14.56	14.70	-0.87	0.41	B1 V	141	141	IMACS f/4	081006
63877	14.78	14.98	-0.87	0.23	B0.2 V	129	166	IMACS f/4	070920
64032	14.98	14.99	-0.91	0.84	B1e ₂₊	–	–	IMACS f/4	090826
64194	14.61	14.60	-0.98	0.99	B0e ₃	168	168	IMACS f/4	090826
64453	13.41	13.38	-1.06	1.14	B1e ₃₊	194	194	IMACS f/4	090826
64710	14.51	14.56	-0.85	0.68	B1.5e ₃₊	117	161	IMACS f/4	081007
64773	15.05	15.25	-0.87	0.23	O8.5 V	136	136	IMACS f/4	090826
65103	15.03	15.09	-0.97	0.74	Be ₂₊	125	125	IMACS f/4	081006
65145	15.11	15.00	-0.85	1.19	B1.5e ₂	175	175	IMACS f/4	081006
65318	14.78	14.95	-0.89	0.35	O9 Ve ₁	190	190	IMACS f/4	081007
65346	14.99	15.19	-0.99	0.36	O8 V	156	163	MIKE	111026
65355	14.71	14.91	-0.92	0.28	O8 V + O9	–	–	IMACS f/4	090826
66160	12.92	13.09	-0.92	0.40	O + B	125	166	IMACS f/4	081006
66302	14.78	14.80	-0.98	0.87	B1e ₃₊	174	174	IMACS f/4	081006
66415	13.08	13.25	-0.91	0.38	O9.7 Ia	166	166	IMACS f/4	081006

Table 1—Continued

ID ^b	B^b	V^b	Q_{UBR}	A_V^c	Sp Type	RV_{star} (km s ⁻¹)	RV_{HI}^d (km s ⁻¹)	Instrument	Observation Date (YYMMDD)
66507	14.83	14.91	-0.96	0.68	B1e ₃ +	–	–	IMACS f/4	081006
67029	15.08	15.21	-0.86	0.40	B1 V	148	141	IMACS f/4	081006
67060	14.43	14.63	-0.94	0.28	O7 Vz	126	164	IMACS f/4	090828
67269	14.56	14.73	-0.93	0.40	O7 V	144	140	IMACS f/4	090826
67305	15.16	15.20	-0.93	0.77	B1.5e ₃	180	180	IMACS f/4	081006
67334	14.93	15.05	-0.94	0.53	B0 V	209	202	IMACS f/4	081006
67673	14.80	14.84	-1.00	0.83	O9.5 V:e ₂	–	–	IMACS f/4	090826
67893	13.92	13.97	-1.05	0.87	B0e ₃ +	–	–	IMACS f/4	081006
68071	14.99	15.19	-0.91	0.28	O9.5 III	177	177	IMACS f/4	081006
68157	15.14	15.37	-0.85	0.10	B0.2 V	204	201	IMACS f/4	081006
68427	13.52	13.51	-1.06	1.09	B0.2e ₄	157	157	IMACS f/4	090826
68621	14.41	14.64	-0.94	0.20	O9.5 III	156	174	IMACS f/4	090828
68756	14.30	14.48	-0.94	0.34	O7.5 III:	205	205	IMACS f/4	090828
68963	15.20	15.39	-0.87	0.25	B0 V	163	163	IMACS f/4	081006
69155	14.50	14.69	-0.85	0.28	B0.2 III	209	206	IMACS f/4	090828
69460	14.82	14.95	-0.99	0.53	O6.5 III((f))e ₂	130	146	IMACS f/4	090826
69555	14.35	14.59	-0.96	0.17	O6.5 V	223	197	IMACS f/4	090826
69598	15.03	15.23	-0.95	0.22	O9 V	175	175	IMACS f/4	090828
69630	13.79	14.01	-0.85	0.16	B1 II	–	–	IMACS f/4	081006
69769	15.13	15.30	-0.93	0.37	B1.5 V	122	131	IMACS f/4	081006
70149	14.41	14.61	-0.90	0.25	O9 V	155	155	IMACS f/4	090826
70663	14.60	14.63	-0.89	0.80	B1.5e ₁	–	–	IMACS f/2	110720
71002	13.75	13.97	-0.93	0.23	O9.5 III	154	163	IMACS f/4	090826
71409	14.91	14.88	-1.05	1.14	Be ₃	–	–	IMACS f/4	090826
71652	14.44	14.65	-0.88	0.18	B0.5e ₂	–	–	IMACS f/4	090825
71815	15.20	15.43	-0.96	0.21	O8 V	172	172	IMACS f/4	090826
72204	14.34	14.57	-0.92	0.20	O8 V + O8 V	–	–	IMACS f/4	090826
72208	12.41	12.54	-0.89	0.48	B1 II	131	133	IMACS f/4	090828
72210	14.47	14.48	-1.02	0.99	B0e ₃	–	–	IMACS f/4	090825
72535	13.42	13.45	-1.11	1.00	O8-9: IIIpe:1	162	162	IMACS f/4	090825
72656	14.85	14.99	-0.85	0.41	B0-1.5 III	135	168	IMACS f/4	090826
72724	14.25	14.42	-0.87	0.34	B0 V	201	201	IMACS f/4	090828
72884	14.65	14.90	-0.92	0.11	O9 V	222	204	IMACS f/4	090826
72941	14.86	15.11	-0.90	0.10	O9 V	110	126	IMACS f/4	090828
73185	15.19	15.27	-0.95	0.72	B	–	–	IMACS f/2	111012
73337	12.96	13.12	-0.96	0.47	O8.5 I((f))	202	202	IMACS f/4	090828
73355	14.26	14.36	-0.93	0.59	B0e ₂	–	–	IMACS f/4	090825

Table 1—Continued

ID ^b	B^b	V^b	Q_{UBR}	A_V^c	Sp Type	RV _{star} (km s ⁻¹)	RV _{HI} ^d (km s ⁻¹)	Instrument	Observation Date (YYMMDD)
73795	14.68	14.73	-1.03	0.82	mid Oe ₃ +	–	–	IMACS f/2	110720
73913	13.57	13.63	-0.91	0.72	O9.5 I	184	184	IMACS f/4	090825
73952	12.51	12.62	-0.88	0.52	B1.5 II	135	135	IMACS f/4	101221
74828	12.97	13.08	-0.86	0.52	Be	–	–	IMACS f/4	090825
74946	15.13	15.14	-0.99	0.88	B	73	131	IMACS f/4	101221
75061	14.17	14.24	-0.93	0.69	B1e ₂	164	164	IMACS f/4	090825
75126	14.65	14.39	-1.14	2.02	O9 V	139	139	IMACS f/4	090825
75210	14.57	14.67	-0.89	0.59	O8.5 V	196	196	IMACS f/4	090825
75626	14.87	15.14	-0.93	0.04	O9 III-V	159	159	IMACS f/4	090825
75689	14.31	14.34	-1.08	0.94	Ope ₃ pec	–	–	MIKE	111025
75719	14.60	14.87	-0.84	0.00	–	–	–	–	–
75919	14.32	14.39	-1.01	0.78	O9 IIIe ₁	166	166	IMACS f/4	101221
75980	14.12	14.17	-1.02	0.81	B0e ₃	–	–	IMACS f/4	090826
75984	15.12	15.35	-0.85	0.07	B0 III	229	212	MIKE	111026
76253	15.04	15.27	-0.90	0.13	B0.2 V + B	188	188	IMACS f/4	090825
76371	13.76	13.96	-0.91	0.30	O9.5 III	–	–	IMACS f/4	090826
76654	14.74	14.75	-1.17	1.04	Be ₃	–	–	IMACS f/4	090826
76657	15.14	15.31	-0.94	0.43	O9-9.5 V	198	198	IMACS f/4	090826
76773	13.46	13.59	-0.86	0.45	Be	–	–	IMACS f/4	090825
76870	14.92	14.98	-0.99	0.77	Be	–	–	IMACS f/2	111013
77290	15.10	15.10	-1.04	1.00	B0.5e ₂ +	–	–	IMACS f/4	090825
77368	13.76	14.00	-0.93	0.15	O6 V	222	202	IMACS f/4	090826
77458	13.00	13.15	-0.92	0.45	B0.2e ₁	204	204	IMACS f/4	090826
77609	12.55	12.69	-0.91	0.48	B0.5 I	192	192	IMACS f/4	090825
77616	14.11	14.08	-1.11	1.22	early Ope ₃ pec	–	–	IMACS f/4	090826
77734	14.87	14.93	-0.97	0.74	–	–	–	IMACS f/4	090826
77816	14.43	14.59	-0.85	0.34	B0.2 III	168	168	IMACS f/4	090825
77851	14.09	14.14	-0.96	0.82	B0.2-1e ₃ +	–	–	IMACS f/4	090826
78438	14.79	15.02	-0.86	0.11	B0 V	–	–	IMACS f/2	110720
78694	14.27	14.35	-0.98	0.72	O8.5 IIIe ₂ +	–	–	IMACS f/2	110721
79225	14.65	14.69	-1.06	0.88	Be ₄ +	150	171	MIKE	111026
79248	14.40	14.60	-0.92	0.29	O8.5 V	–	–	IMACS f/2	110721
79326	14.90	14.94	-0.95	0.80	Be	–	–	IMACS f/2	110719
79513	14.71	14.88	-0.97	0.42	Be	–	–	IMACS f/2	110719
79587	14.98	15.13	-0.87	0.38	B	–	–	IMACS f/2	111012
79697	14.86	14.93	-1.04	0.79	Be ₄	219	201	MIKE	111026
79976	14.74	14.74	-1.01	1.01	Be ₃ +	–	–	IMACS f/2	110720

Table 1—Continued

ID ^b	B^b	V^b	Q_{UBR}	A_V^c	Sp Type	RV _{star} (km s ⁻¹)	RV _{HI} ^d (km s ⁻¹)	Instrument	Observation Date (YYMMDD)
80075	14.90	15.07	-0.87	0.35	B	–	–	IMACS f/2	111012
80352	14.23	14.28	-1.08	0.90	Be	–	–	IMACS f/2	111013
80412	13.33	13.46	-0.94	0.53	B0.7 II	184	150	IMACS f/4	090828
80545	13.36	13.53	-0.89	0.36	B0.5 II	–	–	IMACS f/4	090828
80573	14.38	14.48	-0.85	0.54	B1 V	179	179	IMACS f/4	090827
80579	14.66	14.81	-0.84	0.38	B0.7 V	168	163	IMACS f/4	090827
80582	14.40	14.48	-0.92	0.66	B	–	–	IMACS f/4	090828
80998	14.24	14.46	-0.96	0.25	O8 V	–	–	IMACS f/2	110721
81019	14.24	14.43	-0.93	0.33	O9.5 V	162	162	IMACS f/4	090827
81071	14.67	14.70	-0.99	0.88	Be ₁	–	–	IMACS f/2	110721
81169	15.02	15.23	-0.86	0.19	B0.2 V	178	178	IMACS f/4	090827
81258	14.96	15.18	-0.88	0.14	B0-1.5 V	247	174	IMACS f/4	090827
81465	14.85	14.88	-1.02	0.89	Be ₃	–	–	IMACS f/4	090826
81634	14.42	14.50	-0.86	0.57	B1.5 Ve ₃	177	181	IMACS f/4	090826
81646	14.15	14.36	-0.92	0.26	O8 V	185	185	IMACS f/4	090826
81647	14.62	14.85	-0.89	0.17	B0.2 V	168	168	IMACS f/4	090827
81696	15.07	15.17	-0.91	0.55	B1 V	194	187	IMACS f/4	090826
81941	13.82	14.03	-0.89	0.24	O9.5 III	200	187	IMACS f/4	090827
82322	14.12	14.37	-0.88	0.09	O9.5 III	171	171	IMACS f/4	090827
82328	14.87	14.96	-1.01	0.71	B0e ₂	–	–	IMACS f/4	090826
82387	15.07	15.26	-0.87	0.27	Be	–	–	IMACS f/2	111011
82408	14.39	14.59	-0.87	0.23	B1 III	196	176	IMACS f/4	090826
82444	15.15	15.30	-0.95	0.44	B0 V	199	169	IMACS f/4	090826
82489	14.17	14.22	-1.04	0.86	O9: IIIpe ₄₊	–	–	IMACS f/4	090827
82572	14.45	14.40	-0.85	0.96	Be	–	–	IMACS f/2	111011
82711	14.32	14.36	-1.00	0.83	B1 V	–	–	IMACS f/4	090826
82783	14.88	15.12	-0.89	0.11	B0.5 V	160	160	IMACS f/4	090827
83017	14.80	15.03	-0.87	0.15	O9.5 III	191	181	IMACS f/4	090826
83073	15.10	15.27	-0.87	0.34	B0.7 V	158	215	IMACS f/4	090826
83074	15.12	15.35	-0.85	0.10	Be	–	–	IMACS f/2	111013
83171	14.28	14.39	-0.94	0.58	B0e ₂	–	–	IMACS f/4	090826
83202	12.61	11.53	-0.87	0.47	Be	–	–	IMACS f/2	110719
83224	14.60	14.65	-1.12	0.90	B1e ₃	–	–	IMACS f/4	090826
83232	14.11	14.28	-0.84	0.29	B1.5 III	–	–	IMACS f/4	090826
83480	13.74	13.73	-0.90	0.88	B[e]	164	164	IMACS f/4	090826
83510	15.16	15.45	-0.91	0.00	O8 V	153	159	IMACS f/4	090826
83651	14.88	15.08	-0.86	0.24	B	–	–	IMACS f/2	111012

Table 1—Continued

ID ^b	B^b	V^b	Q_{UBR}	A_V^c	Sp Type	RV_{star} (km s ⁻¹)	RV_{HI}^d (km s ⁻¹)	Instrument	Observation Date (YYMMDD)
83678	12.99	13.18	-0.95	0.36	O8.5 III	166	174	IMACS f/4	090826
83962	14.52	14.61	-0.96	0.65	Be ₂	–	–	IMACS f/2	110720
84277	14.42	14.57	-0.85	0.38	B1e ₁	–	–	IMACS f/2	110720
84544	14.88	15.02	-0.91	0.46	Be ₂	–	–	IMACS f/2	111012

^aThis table is published in its entirety in the electronic edition of the *Astrophysical Journal*. A portion is shown here for guidance regarding its form and content.

^bFrom Massey (2002).

^cFrom Zaritsky et al. (2002).

^dMeasured from Stanimirović et al. (1999).

^eObserved multiple times for binary monitoring; see Table 3.

^fFrom Massey (2012).